

XMM-Newton VIEW OF THE ULTRA-LUMINOUS X-RAY SOURCES IN M 51

GULAB C. DEWANGAN¹, RICHARD E. GRIFFITHS¹, MANOJENDU CHOUDHURY², TAKAMITSU MIYAJI¹, & NICHOLAS J. SCHURCH¹

Draft version June 29, 2018

ABSTRACT

We present results based on *XMM-Newton* observation of the nearby spiral galaxy M 51 (NGC 5194 and NGC 5195). We confirm the presence of the seven known ULXs with luminosities exceeding the Eddington luminosity for a $10M_{\odot}$ black hole, a low luminosity active galactic nucleus with 2–10 keV luminosity of 1.6×10^{39} erg s⁻¹, and soft thermal extended emission from NGC 5194 detected with *Chandra*. In addition, we also detected a new ULX with luminosity $\sim 10^{39}$ erg s⁻¹. We have studied the spectral and temporal properties of the LLAGN and 8 ULXs in NGC 5194, and an ULX in NGC 5195. Two ULXs in NGC 5194 show evidence for short-term variability, and all but two ULXs vary on long time scales (over a baseline of ~ 2.5 years), providing strong evidence that these are accreting sources. One ULX in NGC 5194, source 69, shows possible periodic behavior in its X-ray flux. We derive a period of 5925 ± 200 s at a confidence level of 95%, based on three cycles. This period is lower than the period of 7620 ± 500 s derived from a *Chandra* observation in 2000. The higher effective area of *XMM-Newton* enables us to identify multiple components in the spectra of ULXs. Most ULXs require at least two components – a power law and a soft X-ray excess component which is modeled by an optically thin plasma or multicolor disk blackbody (MCD). However, the soft excess emission, inferred from all ULXs except source 69, are unlikely to be physically associated with the ULXs as their strengths are comparable to that of the surrounding diffuse emission. The soft excess emission of source 69 is well described either by a two temperature *mekal* plasma or a single temperature *mekal* plasma ($kT \sim 690$ eV) and an MCD ($kT \sim 170$ eV). The MCD component suggests a cooler accretion disks compared to that in Galactic X-ray binaries and consistent with that expected for intermediate mass black holes (IMBHs). An iron K α line ($EW \sim 700$ eV) or K absorption edge at ~ 7.1 keV is present in the EPIC PN spectrum of source 26. The spectrum of the ULX in NGC 5195, source 12, is consistent with a simple power law. The LLAGN in NGC 5194 shows an extremely flat hard X-ray power-law ($\Gamma \sim 0.7$), a narrow iron K α line at 6.4 keV ($EW \sim 3$ keV), and strong soft X-ray excess emission. The full band spectrum is well described by a two component *mekal* plasma and reflection from cold material such as putative torus.

Subject headings: accretion, accretion disks — galaxies: active — galaxies: individual (M 51) — X-rays: binaries — X-rays: galaxies

1. INTRODUCTION

X-ray emission from spiral galaxies consists of several components including an active nucleus (if present), extra-nuclear point X-ray sources, hot gas, supernova etc. Many spiral galaxies contain a mildly or non-active nucleus and, in this case, the luminosity in the X-ray band is dominated by the emission from a few luminous off-nuclear point sources (Roberts & Warwick 2000). The brightest of these X-ray sources, with luminosities exceeding the Eddington luminosity for a $10M_{\odot}$ black hole, are defined as the ultra-luminous X-ray sources (ULXs). These objects, which may sometimes individually outshine the rest of the galaxy, were first discovered in *Einstein* observations (Fabbiano & Trinchieri 1987; Fabbiano 1989). Later they were detected in large numbers by *ROSAT* (Colbert & Mushotzky 1999; Roberts & Warwick 2000; Colbert & Ptak 2002). The first detailed X-ray spectral characteristics of ULXs were revealed by *ASCA* and demonstrated that most ULXs exhibit multicolor disk blackbody spectra with a ‘high temperature’

similar to that observed from Galactic X-ray binaries in their high state. Some ULXs were also found to vary and make a transition, at lower luminosities, to power-law spectra, similar to the spectral transitions seen in many Galactic XRBs. However, the observed X-ray flux of many ULXs implies (assuming isotropic emission and Eddington-luminosity limited systems) black holes of $\sim 10^2 - 10^4 M_{\odot}$. These masses are much larger than the measured masses of known Galactic X-ray binaries or black holes (GXRBs or GBHs) and much lower than the measured masses of active galactic nuclei, thus making them candidates for intermediate-mass black holes (IMBHs).

Several models have been proposed to explain the high luminosities of ULXs. These include (i) accreting IMBHs with sub-Eddington rates (e.g., Colbert & Mushotzky 1999), (ii) XRBs with anisotropic emission (King et al. 2001), (iii) beamed XRBs with relativistic jets directly pointing towards us i. e., scaled down versions of blazars (Mirabel & Rodriguez 1999), and (iv) XRBs with super-Eddington accretion rates (Begelman 2002). A few ULXs have been found to be young supernova (e.g., SN 1979, Immler, Pietsch & Aschenbach 1998) with X-ray emission powered by the interactions of shock waves and the surrounding dense inter stellar medium. Some of the

¹ Department of Physics, Carnegie Mellon University, 5000 Forbes Ave, Pittsburgh, PA 15213 USA

² National Center for Radio Astrophysics, Tata Institute of Fundamental Research, Pune 411007, India

accretion-powered ULXs are also observed to be associated with older supernova remnant-like structures (e.g., IC 342-X1, Roberts et al. 2003). The recent observation of a break at a frequency of ~ 28 mHz in the power density spectrum of the ULX NGC 4559 X-7 suggests a mass of a few thousands solar masses, consistent with the measured thermal temperature of $kT = 120$ eV. This observation clearly supports the IMBH scenario for ULXs. It has become increasingly clear that there are two separate populations of ULXs. A large number of ULXs are located in regions of current star formation in star-burst and spiral galaxies (The Antennae, Zezas et al. 2002; NGC 3256, Lira et al. 2002; NGC 4485/90, Roberts et al. 2002; Arp 299, Zezas, Ward, & Murray 2003; M 51, Terashima & Wilson 2004). These ULXs are likely to be associated with young stellar populations. Other ULXs have been observed in early-type elliptical/SO galaxies and are likely to be associated with older stellar populations. A recent study of the ULX population of 82 galaxies by Swartz et al. (2004) suggests that $\sim 25\%$ of these sources may be background objects, including 14% in spiral galaxies and 44% in elliptical galaxies.

Chandra has revolutionized the detection of ULXs primarily due to its superior angular resolution (see e. g., Swartz et al. 2004). *XMM-Newton*, on the other hand, has been probing the detailed characteristics of the ULX populations in nearby galaxies due to its large effective area. *XMM-Newton* is well suited to study detailed spectral and temporal characteristics of ULXs in nearby galaxies (e.g., Strohmayer & Mushotzky 2003; Cropper et al. 2003; Miller et al. 2004; Dewangan et al. 2004).

M 51, also known as the Whirlpool galaxy, is a face-on spiral galaxy and is located at a distance of 8.4 Mpc (Feldmeier et al. 1997). Optical studies of emission lines classified it as a LINER or a Seyfert 2 galaxy (Stauffer 1982). Furthermore, Ho et al. (1997) suggest the presence of a broad $H\alpha$ line. Kohno et al. (1996) found a nuclear molecular disk, and constrained the dynamical mass within 70 pc of the nucleus to be $4 - 7 \times 10^6 M_\odot$. This indicates that M 51 hosts as massive a black hole as many AGNs.

X-ray observations also strongly suggest the presence of an AGN in M 51. *Einstein* (Palumbo et al. 1985) and ROSAT (Marston et al. 1995; Ehle et al. 1995) observations constrained the soft X-ray luminosity of the M 51 nucleus to be $L_X < 5 \times 10^{39} \text{ erg s}^{-1}$. *Ginga* scanning observations in 1988 detected bright hard X-ray emission with 2 – 20 keV luminosity of $\sim 1.2 \times 10^{41} \text{ erg s}^{-1}$, a photon index of 1.43 ± 0.08 and an intrinsic absorption of $< 7 \times 10^{21} \text{ cm}^{-2}$ (Makishima et al. 1990). Such hard nuclear X-ray emission is often considered to be evidence for a low luminosity AGN (LLAGN). *ASCA* observed M 51 in the hard (2 – 10 keV) X-ray band in 1993, and did not detect such a bright hard component. Instead, a faint hard X-ray continuum with a neutral Fe $K\alpha$ line was detected, whose flux was an order of magnitude lower than that measured by *Ginga* (Terashima et al. 1998). The reason for this large difference in luminosity has recently been clarified by *BepposAX* observations. Fukazawa et al. (2001) find that the nucleus is photoelectrically absorbed below 10 keV but is observed directly above 20 keV, implying an absorbing column of $N_H \simeq 5.6 \times 10^{24} \text{ cm}^{-2}$. The 2-10 keV luminosity measured by *BepposAX* was similar to that

of *ASCA*. Fukazawa et al. (2001) attributed the higher *Ginga* luminosity to variability of the absorbing column.

High angular resolution *ROSAT* HRI observations also revealed eight X-ray point sources and diffuse soft X-ray emission in M 51. *Chandra* observed M 51 during June 2000 and June 2001 with ACIS-S. These data have been studied in detail by Terashima & Wilson (2001, 2004). The X-ray image revealed the nucleus, 113 X-ray sources and extended emission which resembled the morphology of both the radio and optical emission line images (Terashima & Wilson 2001). The X-ray image of the nucleus is well represented by a model consisting of soft thermal plasma ($kT \simeq 0.5$ keV), a very hard continuum and an Fe $K\alpha$ emission line at 6.45 keV with an equivalent width of greater than 2 keV. The X-ray spectra of the extra-nuclear clouds are well fitted by a thermal plasma model with $kT \simeq 0.5$ keV. The spectral shape and morphology strongly suggest that the clouds are shock-heated by a bipolar outflow from the nucleus. Out of 113 extra-nuclear sources, 9 sources have luminosities exceeding $10^{39} \text{ erg s}^{-1}$ in the 0.5-8 keV band. The number of extra-nuclear sources in M 51 is much higher than in most other normal spiral and elliptical galaxies and is similar to galaxies experiencing star-burst activity. The X-ray spectra of most of the detected sources are consistent with a power-law spectral form with a photon index between 1 and 2, while one source has an extremely hard spectrum and two sources have particularly soft spectra. The X-ray spectra of three of the ULXs are consistent with both a power-law and multi-color blackbody model. One ULX showed a remarkable spectrum with prominent emission lines.

In this paper we present an *XMM-Newton* EPIC observation of M 51. Utilizing the large collecting area of *XMM-Newton*, we have studied spectral and temporal properties of nine ULXs and the LLAGN in M 51. The paper is organized as follows. In Sect. 2, we outline the observation and the data selection. In Sect. 3, 4, and 5, we present the spatial, temporal, spectral analysis. Sect. 6 describes properties of the individual ULXs. We discuss the results in Sect. 7, followed by conclusions in Sect. 8.

2. OBSERVATIONS AND DATA SELECTION

The galaxy M 51 was observed by *XMM-Newton* observatory (Jansen et al. 2001) on 2003 January 15 for a duration of ~ 21 ks. The EPIC PN (Strüder et al. 2001) and MOS (Turner et al. 2001) cameras were operated in full-frame mode using the thin filter. The optical monitor (OM) instrument and the reflection grating spectrometers operated simultaneously with the EPIC cameras.

The raw PN and MOS events were processed and filtered using the most recent version of the calibration database and analysis software (*SAS v6.0*) available in March 2004. Examination of the background light curves extracted from source-free regions showed that our observations was not strongly affected by particle induced flares. Events in known bad pixels were discarded. For the spectral analysis, we used events with patterns 0–4 (single and double) and flag zero for the PN, and patterns 0–12 (similar to *ASCA* event grades 0–4) and flag zero for the MOS. However, for the temporal analysis, we used all events with pattern 0–12 for both the PN and MOS cameras.

3. SPATIAL ANALYSIS

We extracted PN images in the full (0.2 – 10 keV), 0.2 – 0.7 keV, 0.7 – 2 keV, and 2 – 10 keV bands. First we adaptively smoothed the full band image using the CIAO task *csmooth* and created a smoothing kernel. The images in the 0.2 – 0.7 keV, 0.7 – 2 keV and 2 – 10 keV bands were then adaptively smoothed using the kernel created above, and combined to form a three-color image shown in Figure 1 (*Left*). The color image shows several discrete sources, diffuse soft emission, and the bright nucleus of NGC 5194. Interestingly, the bright nucleus of NGC 5194 actually consists of two hard X-ray sources $\sim 20''$ apart (see below). Also present is the companion galaxy NGC 5195 showing diffuse emission, multiple sources in the central region, and a bright point source to the left of the nucleus. To avoid any possible confusion on multiple source identification numbers arising from multiple X-ray missions, we follow the *Chandra* source identification numbers as set by Terashima & Wilson (2004). Figure 1 (*right*) shows the EPIC PN image in the 2 – 10 keV band and the positions of the ULXs studied in this paper have been marked. The ULX source 9 in NGC 5194 is not seen in the hard band image due to its location in the chip gap and its extreme softness. The source counts and positions listed in Table 1 have been determined by a source detection procedure by utilizing a series of SAS tasks as described by Miyaji et al. (2003). In short, an input image is searched for point-like sources by a simple sliding-cell detection method with local background using *eboxdetect*. This is followed by a “background map” creation by a spline fit to the source-excluded region using *esplinemap*. A sliding cell detection is repeated to find excess over this background map (*eboxdetect*). The final source positions and counts are determined by a multi-source maximum-likelihood fit with the *XMM-Newton* PSF, using the sources detected in the previous step as the starting points (*emldetect*). In order to be free from the effects of soft diffuse emission, which could prevent the accurate determination of the background map, the hard-band (2-10 keV) image is used to obtain the source counts, except source 9, which has not been detected in the hard band. In Figure 2, we show the UV image of M 51 taken with the *XMM-Newton* OM. The image shows beautiful spiral arms, a prominent nucleus, and bright star clusters surrounding the nucleus with either a ring-like morphology or multiple inner spiral arms. One of the spiral arm of NGC 5194 appears to be tidally connected to the companion galaxy NGC 5195. This galaxy shows a bright nucleus with dark dust lanes near the nucleus.

In Fig. 2, we have overlaid the X-ray contours onto the UV image. The contours represent the hard (1.5 – 12 keV) X-ray sources only. Fig. 2 highlights the two bright hard X-ray sources in the central region of NGC 5194. The two sources are separated by $\sim 20''$. The fainter of the two X-ray sources coincides with the UV nucleus. The brighter source is an ULX, which is clearly resolved in *Chandra* images (Terashima & Wilson 2004).

In this paper we study the active nucleus and the point sources with luminosities $\geq 10^{39}$ erg s $^{-1}$ in the 0.3 – 12 keV band. There are eight ULXs in addition to the LLAGN in NGC 5194. There is also a well iso-

lated ULX in the companion galaxy NGC 5195. However, the central region of NGC 5195 consists of multiple bright point sources and extended soft emission as seen in the *Chandra* ACIS-S image (Terashima & Wilson 2004). Due to lower angular resolution of *XMM-Newton*, it is not possible to extract counts for individual sources in the central region of NGC 5195. Therefore we exclude the bright sources in the central region of NGC 5195 from our analysis. The *Chandra* source NGC 5194#63 had an X-ray luminosity $< 10^{39}$ erg s $^{-1}$ during the two previous *Chandra* observations. In this observation this source has a luminosity of $\sim 2 \times 10^{39}$ erg s $^{-1}$ in the 0.3 – 10 keV band and we now include this source in our sample.

4. TEMPORAL ANALYSIS

4.1. Short-term variability

We extracted 0.2 – 12 keV X-ray light curves for the LLAGN and ULXs in M 51 from the EPIC PN data. The extraction regions had radii in the range of 15 – 35'' and enclosed $> 60\%$ of the X-ray emission from each source. The smallest circular regions were chosen to avoid contamination from nearby sources. We used time bins of 520 s and required that the bins be at least 50% exposed in order to minimize the errors due to the low number of counts from the weak sources. We also extracted individual background light curves for each of the sources using circular regions lying approximately at the same readout distance as that for the source. The source light curves were then corrected for the background contribution using the background light curves and appropriate scaling factors to take into account the different extraction areas.

We fit a constant count rate model to each of the light curves to investigate the possibility of rapid variability. We rebin the light curves, if required, to ensure a minimum of 20 counts per bin to allow the use of χ^2 fitting statistics. The results for each light curve are listed in Table 2. We find that only two of the sources show significant variability: source 26 (at the 98.6% confidence level) and source 69 (99.95% confidence level). The light curves of these two sources are plotted in Figure 3.

4.2. Periodicity

Source 69 shows the most significant rapid variability. The light curve shows three tentative peaks at regular intervals. The first *Chandra* observation of this ULX in June 2000 showed two peaks separated by ~ 7000 s. These features were interpreted by Liu et al. (2002) as a signal with a period of ~ 2.1 hr. We have searched for a similar periodic signal in the *XMM-Newton* light curves. For this purpose, we combined the PN and MOS light curves, binned to 520 s. The initial search for periodicity in the source, as well as the folding of the light curve with respect to the final period obtained was performed with the XRONOS 5.19 package, which is a part of FTOOLS 5.2. The periodogram was obtained using the algorithm of Scargle (1982), following the recipe of normalizing the periodogram power using the total variance of the complete light curve as prescribed by Horne & Baliunas (1986). This algorithm is very robust for detecting periodic signals in light curves with few data points as well as non-uniformly distributed observational data, while providing a ‘false alarm probability’ of the periodicity arising in the light curve from random noise.

This probability is obtained using the signal to noise ratio, where the variance of the noise is obtained under the basic assumption that it is a normally distributed random variable. The periodogram is shown in Figure 4 (*left*). The period obtained was 5925 ± 200 s, with a 'false alarm probability' of 0.045, suggesting that the observed modulation is not generated by the statistical fluctuation of the noise, to a confidence level of 95.5%. The main source of the noise in the power in the Fourier frequency domain are the inherent statistical fluctuations at scales < 2 ks (Figure 4). We have tested for the periodicity on top of a constant count rate. However, in reality, the source probably has a red-noise power spectrum, similar to XRBs. Therefore, the $\sim 2\sigma$ or 95.5% detection of the period is an upper limit, and the periodicity may or may not be a true signal. Future long baseline X-ray observations will be crucial for the robust detection of the periodicity from this ULX. In Figure 4 (*right*) we provide the light curve folded with respect to the period of 5925 s, with a bin size of 520 s. Evidently, the modulation fraction is in excess of 45%, similar to the estimate of Liu et al. (2002).

4.3. Long-term Variability

We have compared the 0.5 – 8 keV fluxes derived from the *XMM-Newton* observation (see below) and earlier two observations with *Chandra* (Terashima & Wilson 2004) in June 2000 and June 2001. Figure 5 shows the comparison of the fluxes. Cross-calibration results suggest that the fluxes measured with *Chandra* and *XMM-Newton* agree at a level better than 10% (Snowden 2002). Thus, all the ULXs, except NGC 5194#41 and NGC 5195#12, show long-term significant variability over a baseline of 2.5 yr.

5. SPECTRAL ANALYSIS

For each ULX and the LLAGN, we extracted source and background spectra from the final filtered PN event list using the same extraction regions that we used for the PN light curves. We also extracted the source spectra from the MOS data using source regions similar to that used for the PN. The background MOS spectra for the individual ULXs were extracted using circles in the nearby source-free regions. Appropriate PN and MOS responses and effective area files were created for each source using the SAS tasks *rmfgen* and *arfgen*. A grouping of 20 counts per spectral channel resulted in significant degradation in the spectral resolution of the ULX spectra above 2 keV. Therefore, all the source spectra were grouped to a minimum of 10 counts per spectral channel so that discrete spectral features are not missed. The spectra were analyzed with the XSPEC 11.3 spectral analysis package (Arnaud 1996), and using the C-statistics instead of χ^2 -statistic which is not useful in the case of low ($\lesssim 20$) counts per bin. Unlike the χ^2 -statistic, the C-statistic does not provide a goodness-of-fit (GOF) criterion. Therefore we simulate 5000 spectra based on the best-fit model derived using the C-statistic, and calculate the percentage of these spectra with the C-statistic less than that for the data. This number provides the GOF, and if this number is $\sim 50\%$, then the model is a good fit to the observed spectrum (similar to the reduced $\chi^2 \sim 1$ criterion), though obviously we cannot statistically exclude fits for which $\text{GOF} \leq 95\%$. The

confidence intervals are calculated in the same way as in the case of χ^2 -statistic. All the errors quoted below were calculated at 90% confidence level for one interesting parameter i.e., $\Delta C = 2.7$.

At first the MOS and PN spectra of a few bright sources were fitted separately to check for the possible uncertainties due to cross-calibration problems. We found generally good agreement between MOS and PN cameras in the 0.3 – 10 keV bands. Therefore we present the spectral results obtained by fitting the same model jointly to the PN and MOS data while leaving the relative normalizations to vary.

5.1. The low luminosity AGN in NGC 5194

An absorbed power-law model is a poor fit to the PN and MOS spectra of the nucleus of NGC 5194 ($C = 4117.2$ for 409 degrees of freedom (dof), $\text{GOF} = 100.0\%$). To show the significant spectral features, we fitted the absorbed power-law model in the 3 – 5 keV and 7 – 10 keV bands and plotted the ratio of the observed data in the 0.3 – 10 keV band and the best-fit power-law in Figure 6. A strong soft X-ray excess below 1.5 keV and a narrow iron $K\alpha$ line at 6.4 keV are evident in the spectrum. The X-ray image, shown in Fig. 1, clearly shows presence of extended emission which we interpret as originating from optically thin thermal plasma. Accordingly, we added a *mekal* component to describe the soft component and a Gaussian line model at 6.4 keV. The fit improves significantly ($C = 452.3$ for 404 dof, $\text{GOF} = 88.5\%$), however, the soft X-ray emission is not well described. There are still line-like residuals below 2 keV, suggesting either the hot gas responsible for the soft excess emission has a temperature structure and/or its abundance ratio is non-solar. Including an additional *mekal* component (model 1) further improves the fit ($C = 414.7$ for 401 dof; 47.8%), and removes the soft residuals seen earlier. The best-fit temperatures are $kT = 171^{+23}_{-29}$ eV and $kT = 610^{+16}_{-14}$ eV, and the best-fit abundances, relative to solar, are $0.20^{+2.49}_{-0.14}$ and $0.18^{+0.05}_{-0.02}$ for the two *mekal* components. The observed data, the best-fit model and their ratio are plotted in Figure 7. We also tested the possibility of the non-solar abundance ratio by replacing the two *mekal* component by a *vmekal* component (model 2) which allows the abundance ratios of individual elements to vary. This model also improved the fit over that involving a single *mekal* component. The best-fit parameters for both models are listed in Table 3. Model 1 and 2 describe the data statistically equally well ($\text{GOF} = 48\%$, and 47% for model 1 and 2, respectively). Both models result in an extremely flat hard X-ray slope (< 0.8), and strong iron $K\alpha$ line ($\text{EW} \sim 3$ keV) from neutral material.

The flat spectrum and strong iron line strongly suggest that the hard X-ray emission from the LLAGN in NGC 5194 is dominated by reflection from a cold material. Previous *BeppoSAX* observations of M 51 showed the LLAGN is obviously Thomson thick ($N_H = 5.6^{+4.0}_{-1.6} \times 10^{24} \text{ cm}^{-2}$; Fukazawa et al. 2001). Therefore, we replaced the simple power-law model with the Compton reflection model *pekrav* (Magdziarz & Zdziarski 1995). This model calculates the reflected spectrum from a neutral disk exposed to an exponentially cutoff power-law spectrum. Since *XMM-Newton* does not cover the expected peak (20–40 keV) of the reflection component,

it is not possible to tightly constrain all the parameters of the reflection model using this data alone. Instead, we fix the power-law photon index at 1.9, cutoff energy of the primary power law at 200 keV, disk inclination at 70 degrees and the abundance of heavy elements at 0.1 relative to solar value. We also fixed the relative amount of reflection, $R = 1$, corresponding to an isotropic source above a reflecting plane. The only variable parameter of the pexrvt model was the normalization of the incident power law. We chose a high inclination angle due to the Thomson-thick nature of the LLAGN. We also set the reflection model to produce the reflection component alone. This corresponds to a situation in which the primary X-ray emission is completely absorbed by a column density in excess of $\sim 10^{24} \text{ cm}^{-2}$ along the line of sight and we observe the X-ray emission scattered by the matter near the nucleus. We also include a narrow Gaussian line model to describe the Fe K emission. Fitting the above model (model 3) resulted in no strong apparent residuals. Model 3 consisting of two *mekal* components, Compton reflection, and a narrow Gaussian resulted in $C = 420.9$ for 400 dof and $GOF = 61.8\%$. We consider this model to be the best-fit model as it is more physical than the earlier model involving simple power-law. The best-fit *mekal* temperatures are $177^{+36}_{-32} \text{ eV}$, $614^{+13}_{-11} \text{ eV}$. The iron line equivalent width is $2.5^{+1.4}_{-1.4} \text{ keV}$, similar to that measured from *Chandra* observations (Levenson et al. 2002). The best-fit parameters are listed in Table 3 (Model 3). The observed flux is $8.2 \times 10^{-13} \text{ erg s}^{-1}$ in the 0.3 – 10 keV band, and $2.0 \times 10^{-13} \text{ erg s}^{-1}$ in the 2 – 10 keV band, which correspond to luminosities $6.9 \times 10^{39} \text{ erg s}^{-1}$ in the 0.3 – 10 keV band, and $1.7 \times 10^{39} \text{ erg s}^{-1}$, respectively.

5.2. ULXs in M 51

We performed joint fits for the PN and MOS spectra of each ULX with the following spectral models: (i) a power law (PL), (ii) multicolor accretion disk blackbody (MCD), (iii) thermal plasma (*mekal*), (iv) PL+MCD, (v) PL+*mekal*. The models also incorporate photoelectric absorption (*wabs* with a minimum value of $1.5 \times 10^{20} \text{ cm}^{-2}$, the Galactic absorption in the direction of M 51; Stark et al. 1992). We assume an abundance of 0.1 relative to the solar in all the *mekal* components. The point spread function for the two sources 82 and 37 partially coincide with PN CCD chip gaps and/or bad pixel columns, prompting us to restrict ourselves to using only MOS data for the spectral analysis of these sources. One or more of the above models provided a reasonably good fit to all the ULXs except for sources 9, 26 and 69. The best-fit models and the unfolded X-ray spectra of these ULXs are shown in Figure 8. The best-fit parameters are listed in Table 4. We have also listed the 0.5 – 8 keV observed flux and luminosity for the PN data in Table 4. The errors on flux were estimated at 90% level based on 1000 sets of parameter values drawn from the distribution that is assumed to be multivariate Gaussian centered on the best-fit parameters with sigmas from the covariance matrix. The fluxes measured with PN and MOS cameras are within the 90% errors quoted in Table 4. The *mekal* model alone does not provide a good fit to the spectra of all ULXs except source 12, therefore the best-fit parameters are not listed in Table 4.

X-ray spectra of sources 5, 37 and 41 in NGC 5194 are

equally well described by a PL+MCD or a PL+*mekal* model, while source 63 prefers PL+*mekal* model. Two ULXs source 82 in NGC 5194 and source 12 in NGC 5195 only requires a single spectral component. Source 82 is described by a simple power law and does not statistically require any soft component at a level $\geq 99\%$. Source 12 is well described either by a simple power law or a *mekal* model. In Table 4, we have listed the reduction in the C-statistic value (ΔC) for Δp additional parameters for the addition of a soft component (*mekal*, MCD or both, see below) to the simple power-law model. We have also listed the statistical significance derived from the maximum likelihood ratio (MLR) test. The 99% criterion for selecting the more complex model is significance < 0.01 . As a caveat we note that the MLR test is statistically not robust in cases that involve testing a hypothesis that is on the boundary of the parameter space e.g., the null values of the normalizations of MCD, *mekal* and Gaussian lines occur in the simple power law model (Protassov et al. 2002). The results of the MLR test presented here should be treated only as indicative.

The spectra of sources 9, 26 and 69 are not satisfactorily described by any of the four models mentioned above. Source 9 is the softest ULX in our sample. Although not a good fit, the PL+MCD model is marginally better than the PL+*mekal* model for this ULX (see Table 4). Adding a *mekal* component to the PL+MCD model improves the fit ($\Delta C = -9.7$ for two additional parameters), and results in a good fit ($C = 59.8$ for 50 dof, $GOF = 46.9\%$). Replacing the MCD component by another *mekal* component in the PL+MCD+*mekal* model slightly worsened the fit ($C = 67.9$ for 51 dof; $GOF = 78.2\%$).

The ULX source 26 is located in the region of strong, extended soft X-ray emission. Its X-ray spectrum is not well described either by a simple power law or an optical thin plasma. Similar to the spectral modeling of the LLAGN, we used multiple *mekal* components to describe the soft emission. Two *mekal* components are statistically required to explain the soft X-ray excess emission. The addition of the second *mekal* component is significant at a level $> 99.99\%$ ($\Delta C = -28$ for two additional parameters). In Figure 9, we show the ratio of the EPIC data and the best-fit model consisting of two *mekal* components and an absorbed power-law. An iron $K\alpha$ line at $\sim 6.4 \text{ keV}$ is clearly seen in the spectrum. The addition of a Gaussian line improves the fit ($\Delta C = 19.2$ for three additional parameters). The best-fit resulted in $C = 278$ for 295 dof ($GOF = 9.3\%$). The observed EPIC data, the best-fit model and their ratio are plotted in Figure 10. The best-fit parameters are listed in Table 5.

The above fit clearly shows the presence of a Gaussian line. The best-fit line parameters are $E_{\text{line}} = 6.33^{+0.11}_{-0.13} \text{ keV}$, $\sigma = 158^{+180}_{-155} \text{ eV}$, line flux $f_{\text{line}} = 2.3^{+1.5}_{-1.2} \times 10^{-6} \text{ photons cm}^{-2} \text{ s}^{-1}$ and $EW = 550 \text{ eV}$, consistent with an iron $K\alpha$ line from neutral material. The LLAGN in NGC 5194, a Compton-thick AGN, also shows strong ($EW \sim 3 \text{ keV}$; see also Levenson et al. 2002). The ULX NGC 5194#26 is separated by only $28''$ from the LLAGN. The fractional encircled energy for the PN is $\sim 80\%$ at a radius of $28''$. The location of NGC 5194#26 within the wings of the point spread function and the very strong narrow iron line of LLAGN raise doubt if the iron $K\alpha$ emission inferred from the ULX is sim-

ply cross-contamination from the LLAGN. To investigate this possibility, we extracted a background spectrum using circular regions with centers at the same distance from the LLAGN as that of NGC 5194#26. The radii of the two circles were chosen to be the same as that of the circular region used to extract the spectrum of NGC 5194#26. We used the PN data only and carried out the spectral analysis in the 2 – 10 keV band. A simple absorbed power-law model provided $C = 83.8$ for 77 dof and $GOF = 57.0\%$. Addition of a Gaussian line improved the fit ($\Delta C = -13.4$ for three additional parameter). The best-fit parameters are $\Gamma = 2.4_{-0.5}^{+0.5}$, $n_{PL} = 3.0_{-1.8}^{+0.5} \times 10^{-4}$ photons $\text{cm}^{-2} \text{s}^{-1} \text{keV}^{-1}$, $E_{line} = 6.3_{-0.2}^{+0.2}$ keV, $\sigma = 210_{-140}^{+380}$ eV, $f_{line} = 2.7_{-1.5}^{+2.7} \times 10^{-6}$ photons $\text{cm}^{-2} \text{s}^{-1}$, $EW = 690$ eV. Replacing the Gaussian line with an accretion disk line (the *diskline* model in XSPEC) resulted in $C = 69.5$ for 74 dof. The best-fit parameters are $E_{line} = 6.3_{-0.4}^{+0.3}$ keV, disk inclination angle, $i = 26_{-26}^{+32}$ degree, $f_{line} = 3.9_{-1.9}^{+2.3} \times 10^{-6}$ photons $\text{cm}^{-2} \text{s}^{-1}$. The emissivity index, inner and outer radii were kept fixed at -2.5 , $6r_g$ and $1000r_g$, respectively, where r_g is the gravitational radius. The addition of the diskline to the simple power law model improved the fit at a significance level of 99.7%. We also tested if the broad iron line-like feature could be described in terms of an absorption edge. Addition of an edge at ~ 7.1 keV to the absorbed power-law model improved the fit ($C = 70.6$ for 75 dof). The best-fit parameters are $N_H = 2.5_{-2.3}^{+2.1} \times 10^{22} \text{cm}^{-2}$, $\Gamma = 1.2_{-0.6}^{+0.6}$, edge energy $E_{edge} = 7.1_{-0.1}^{+0.2}$ keV and $\tau = 1.4_{-0.6}^{+0.8}$. Thus the 2 – 10 keV EPIC PN spectrum of source 26 is equally well described by an absorbed power law and a broad iron line at ~ 6.3 keV or an iron K-edge at ~ 7.1 keV. It is still possible that the background correction, we adopted here, may not be accurate due to poor signal-to-noise of the data, the presence of extended X-ray emission and moderate spatial resolution of *XMM-Newton*. Future long X-ray observations with *Chandra* and *XMM-Newton* will help detecting the line and/or edge unambiguously.

Source 69 is located in a region of extended soft X-ray emission in an spiral arm. It is likely that X-ray emission from source 69 is contaminated by the extended emission. Adding another *mekal* component to the PL+*mekal* model improved the fit significantly ($\Delta C = 52.7$ for two additional parameters; $C = 191.9$ for 200 dof; $GOF = 18\%$). The best-fit parameters are listed in Table 4. Replacing one of the *mekal* component by the MCD component slightly worsened the fit ($C = 200.9$ for 199 dof, $GOF = 29.2\%$). However, both the fits are acceptable. The spectral data and the best-fit model PL+*mekal*+*mekal* are plotted in Figure 8.

We compared the soft excess flux in the 0.3 – 2 keV band, modeled as *mekal* component above a power-law, of ULXs with that of the diffuse emission in the surrounding regions. We estimated the flux of the diffuse emission from the count rates measured in annular regions centered at the source positions or nearby circular regions. We used the best-fit *mekal* temperature, estimated from the PL+*mekal* model for an ULX, to convert the appropriately scaled count rate of the nearby diffuse emission into the flux in the 0.3 – 2 keV. For all ULXs except source 69, the nearby diffuse emission

is comparable to the soft excess emission, suggesting that the soft excess emission may not be associated with these ULXs. The soft excess emission of source 69 ($f_{mekal} \sim 6.6 \times 10^{-14} \text{erg cm}^{-2} \text{s}^{-1}$) is about a factor of four stronger than the surrounding diffuse emission in the 0.3 – 2 keV band. Thus, at least a part of the soft excess emission is intrinsic to the ULX.

5.2.1. The comptonized accretion disk model

The power law and the MCD model used to fit the ULX spectra above are only a mathematical approximation of the real physical spectra and do not provide much physical insight. Therefore, we also tried a spectral model based on ‘real’ physics of an accretion disk-corona system. This model called as the ‘comptonized accretion disk (CMCD)’ has been used to describe the spectra of six bright ULXs (Wang et al. 2004). The CMCD model was constructed by Yao et al. (2003). The model assumes a thermal energy distribution for electrons in a spherical corona around an accretion disk. The parameters of the CMCD model are the radius of the spherical corona (R_c), electron temperature (T_c), coronal optical depth (τ_c), the temperature of the inner accretion disk (kT_{in}), and disk inclination angle (i). The model is implemented as a standard XSPEC table model (see Yao et al. 2003 and Wang et al. 2004 for more details).

We fitted the CMCD model to the spectra of all the ULXs. It was not possible to constrain the parameters for all but one ULX source 26, due to poor signal-to-noise and/or best-fit parameters outside the tabulated ranges. Due to the contamination of the extended soft X-ray emission, source 26 statistically required two *mekal* components in addition to an absorbed CMCD model. The addition of the first and second *mekal* components improved the fit by $\Delta C = -491.1$ and -19.1 , respectively, for three additional parameters in each case. The *mekal* temperatures are similar to that derived earlier using the combination of two *mekal* and a power law model. The best-fit parameters are listed in Table 5. For the best-fit CMCD model, the inner disk temperature is 291_{-82}^{+93} eV. The disk inclination angle is poorly constrained.

6. INDIVIDUAL ULX CHARACTERISTICS

In this section we describe the X-ray properties of individual ULXs.

6.1. NGC 5194 source 5

This source is located in the western outer spiral arm of NGC 5194, coincident with the *ROSAT* HRI source 4 (Ehle et al. 1995). *Chandra* resolved this source into two discrete sources NGC 5194#5 (CXOM51 J132939.5+471244) and NGC 5194#6 (CXOM51 J132940.0+471237). NGC 5194#5 is brighter than NGC 5194#6 by factors of 1.5 and 11 in the 0.5 – 8 keV and 2 – 8 keV bands, respectively (Terashima & Wilson 2004). Our *XMM-Newton* spectrum of this source requires a soft X-ray excess component that is equally well described either by an MCD or a *mekal* component. This soft excess component contributes $\sim 42\%$ to the total flux in the 0.5 – 2 keV. Therefore, the detection of soft X-ray excess emission above the power-law component in the *XMM-Newton* spectrum could be due to the contamination of the

softer NGC 5194#6 and the ULX spectrum is likely to be a simple power-law.

6.2. NGC 5194 source 9

This is the softest ULX in M 51 (see Fig. 1). This source is coincident to the *ROSAT* HRI source 5 (Ehle et al. 1995) and *Chandra* source NGC 5194#9 which was a super-soft source (Terashima & Wilson 2004). *Chandra* detected no photons above 1 keV from NGC 5194 source 9 and its spectrum was well described by an MCD model with $kT \sim 100$ eV. *XMM-Newton* EPIC MOS detected this source at 6σ and 3σ levels above 1 keV and 2 keV, respectively. The MOS spectra of this source statistically require three components: a power-law ($\Gamma \sim 1.4$), an MCD ($kT \sim 130$ eV), and a *mekal* ($kT \sim 340$ eV). Alternatively, the MOS spectra can also be described by a power law ($\Gamma \sim 1.6$) and two *mekal* components ($kT \sim 80, 306$ eV). The X-ray flux of source 5 was a factor of ~ 3 higher during our *XMM-Newton* observation than that during the *Chandra* observations. The soft X-ray excess (MCD + *mekal*) flux is 7.4×10^{-14} erg cm $^{-2}$ s $^{-1}$ in the 0.5 – 8 keV band which is similar to the total flux observed by *Chandra* in June 2001.

6.3. NGC 5194 source 26

This is the nearest ULX to the LLAGN in NGC 5194. It is located about 28'' west of the LLAGN and its soft X-ray emission is heavily contaminated by extended soft emission. This source was not detected in the *ROSAT* HRI possibly due to the extended soft X-ray emission. This ULX is brighter than the LLAGN in the 1.5–10 keV band (see Fig. 2). *Chandra* also detected this source as the hardest ULX in M 51 (Terashima & Wilson 2004). In the two *Chandra* observations, this source showed interesting spectral behavior. The first *Chandra* observation revealed an absorbed power-law spectrum and emission lines at ~ 1.8 keV, 3.24 keV, ~ 4.03 keV, and ~ 6.65 keV, most likely the $K\alpha$ lines of Si, Ar, Ca, and Fe, respectively (Terashima & Wilson 2004). In the second *Chandra* observation, no emission lines were clearly detected although the source was brighter by $\sim 50\%$. The *XMM-Newton* spectra of this source are well described by an absorbed power-law ($\Gamma \sim 2.4$, $N_H \sim 7.1 \times 10^{22}$ cm $^{-2}$) and two *mekal* components ($kT \sim 250$ eV, ~ 590 eV). The absorbed power-law is consistent with that observed by the second *Chandra* observation. The two *mekal* components represent the contribution of the extended soft emission. We do not detect any emission lines except the iron line or an edge. Future deep X-ray observations will establish if the line is real. The EPIC PN spectrum of source 26, after appropriately correcting for the contribution of extended emission, requires either a moderately broad ($\sigma \sim 200$ eV) iron $K\alpha$ line or a strong iron K edge at ~ 7.1 keV.

6.4. NGC 5194 source 37

This source is coincident with a southern spiral arm of NGC 5194 that displays extended UV emission (see Fig. 2). This source was not detected in the first *Chandra* observation but was detected in the second observation (Terashima & Wilson 2004). During our *XMM-Newton* observations, the ULX was $\sim 50\%$ brighter than dur-

ing the second *Chandra* observation. The *Chandra* spectrum was described by a simple power law, while the *XMM-Newton* spectra statistically require a soft component that is equally well described by a *mekal* or an MCD component, in addition to a power law. The power law is flatter ($\Gamma = 0.8^{+0.4}_{-0.5}$) than that derived from the *Chandra* data ($\Gamma = 1.55^{+0.19}_{-0.15}$). It is likely that this discrepancy is attributable to the different number of spectral components used to describe the *Chandra* and *XMM-Newton* spectra.

6.5. NGC 5194 source 41

This ULX is closer to the nucleus of NGC 5195 than to the nucleus of NGC 5194 but may be associated with the outer edge of an outermost spiral arm to the north of the nucleus of NGC 5194. This source was also detected in the *ROSAT* HRI (source 10 in Ehle et al. 1995). *Chandra* resolved this source into two sources NGC 5194#41 (CXOM51 J132953.7+471436) and NGC 5194#42 (CXOM51 J132953.8+471432). NGC 5194#41 is a factor of ~ 2 more luminous than NGC 5194#42. Remarkably, the *XMM-Newton* source is fainter by $\sim 50\%$ than the *Chandra* source NGC 5194#41 alone. *Chandra* spectra of this ULX are consistent with either a power-law or an MCD and no variability between the two observations. *XMM-Newton* spectra statistically require either an MCD ($kT \sim 270$ eV) or a *mekal* ($kT \sim 340$ eV) in addition to a power-law. Since the *Chandra* source NGC 5194#42 is an absorbed source, the thermal component inferred from the *XMM-Newton* data is likely a genuine component.

6.6. NGC 5194 source 63

This is faintest ULX in M 51 with a 0.5 – 8 keV luminosity of $\sim 10^{39}$ erg s $^{-1}$. This source was fainter by a factor of ~ 2 in the 0.5 – 8 keV band during the *Chandra* observations and was not considered to be a ULX. We consider this source to be a ULX at its increased flux. It is possible that the source is a stellar mass black hole accreting at or near the Eddington rate. The ULX is located to the south-east region coincident with a spiral arm, displaying extended UV emission. The X-ray spectrum of this source shows soft excess emission above a power law ($\Gamma \sim 2.0$) and is statistically better described by a *mekal* plasma than an MCD. The presence of an extended UV source and optically thin thermal plasma both suggest that this ULX may be associated with a region of strong star-formation or unusually X-ray bright supernova remnant.

6.7. NGC 5194 source 69

This ULX is well known for the tentative detection of a 2.1 hr periodicity in its X-ray flux (Liu et al. 2002). It is located in a region of extended soft X-ray emission and strong UV emission in an spiral arm to the north-east of the nucleus. The ULX is closer to the nucleus of NGC 5195 than to the nucleus of NGC 5194 but is clearly associated with NGC 5194. This source was detected in the *ROSAT* HRI (Ehle et al. 1995). The ULX showed drastic long term X-ray variability, its 0.5 – 8 keV luminosity declining by a factor of ~ 75 from the first to the second *Chandra* observation. During our *XMM-Newton* observation, the ULX had brightened by a factor of ~ 50

in the 0.5 – 8 keV band. Source 69 also shows variability on short-times scales. The first *Chandra* observation tentatively detected two peaks separated by ~ 7000 s. Liu et al. (2002) interpreted these features as a 2.1 hr periodicity. The number of counts was too low to detect any such periodicity during the second *Chandra* observation. During a bright flux state during the *XMM-Newton* observation, the source again shows three possible peaks separated this time by ~ 6000 s. We detect a periodic signal at a significance level of 2σ with a period of 5925 ± 200 s from the EPIC light curves (see section 7.2.4 for further discussion). The *XMM-Newton* spectrum of this source is well described by either of the following three component models: (i) a power law ($\Gamma \sim 1.2$) and two *mekal* components ($kT \sim 180$ eV, 680 eV); (ii) a power law ($\Gamma \sim 1.2$), an MCD ($kT \sim 170$ eV), and a *mekal* ($kT \sim 690$ eV).

6.8. NGC 5194 source 82

This is the brightest ULX in M 51 with an observed luminosity of $\sim 2.2 \times 10^{39}$ erg s $^{-1}$ in the 0.5 – 8 keV band. The ULX is coincident with an outer spiral arm east of the nucleus. This source was previously detected with Einstein HRI (Palumbo et al. 1985), *ROSAT* HRI (source 14 in Ehle et al. 1995), *BeppoSAX* (Fukazawa et al. 2001), and *Chandra* (Terashima & Wilson 2004). The source had dimmed in the second *Chandra* observation but was brighter by 35% in the *XMM-Newton* observation, a level similar to that seen during the first *Chandra* observation. Both *Chandra* and *XMM-Newton* spectra of this ULX are consistent with an absorbed power law.

6.9. NGC 5195 source 12

This is the only ULX in NGC 5195 that is well separated from the nucleus. The ULX is $\sim 70''$ away to east of the nucleus. The ULX was earlier detected with the *ROSAT* HRI (source 13 in Ehle et al. 1995). Source 12 is the only ULX in M 51 to have X-ray spectrum that is well described by a single spectral component either a simple power-law ($\Gamma \sim 1.6 \pm 0.2$) or *mekal* plasma ($kT \sim 7.7$ keV). The ULX is not resolved spatially with *Chandra*. Modeling the spectrum as an optically thin plasma requires an unrealistically high temperature and, as a result, we prefer the non-thermal power-law interpretation despite the equally good spectral fits. The notable lack of an optical/UV counterpart for the source strongly suggests that this source is not a background AGN, particularly given its low intrinsic X-ray absorption ($N_H \sim 5.6 \times 10^{20}$ cm $^{-2}$).

7. DISCUSSION

We have performed the temporal and spectral analysis of the LLAGN and nine ULXs in M 51 using a *XMM-Newton* observation. Below we discuss the main results obtained.

7.1. The LLAGN of NGC 5194

The X-ray spectrum of the LLAGN is a typical of Thomson-thick Seyfert 2 galaxies, namely an extremely flat continuum, a strong and narrow line from neutral iron, and unabsorbed soft X-ray emission. Our spectral modeling shows that the flat continuum can be described as the reflection of the primary power-law ($\Gamma = 1.9$) by

cold and dense material, assuming the cold material subtends a 2π solid angle to the central source, the luminosity of the primary continuum is then estimated to be $\sim 10^{40}$ erg s $^{-1}$ in the 0.3 – 10 keV band. This luminosity is about two orders of magnitude lower than that for Seyfert 1 galaxies, thus confirming the nucleus of NGC 5194 as an LLAGN as already established with previous *BeppoSAX* and optical observations. Since the LLAGN is nearly Thomson thick, the soft X-ray emission in the spectrum must be associated with the extended soft emission seen in Fig. 1.

7.2. ULXs in M 51

There are nine ultra-luminous X-ray sources in M 51 with the observed luminosity of $\gtrsim 10^{39}$ erg s $^{-1}$ in the 0.5 – 8 keV band. Three ULXs, source 9, 41 and 63, with $L_X \sim 10^{39}$ erg s $^{-1}$ (0.5 – 8 keV) may actually be stellar mass black holes ($\sim 10 - 20 M_\odot$). The brightest ULX in M 51, source 82, has a 0.5 – 8 keV luminosity of 2.2×10^{39} erg s $^{-1}$, lower than the Eddington luminosity ($\simeq 2.6 \times 10^{39}$ erg s $^{-1}$) for a $20 M_\odot$ black hole. Thus, all ULXs in M 51 could plausibly be stellar mass black holes at around (or slightly above) the Eddington limit.

The larger collecting area of *XMM-Newton* compared to *Chandra* has enabled us to investigate the nature of ULXs in greater detail. While *Chandra* spectrum of individual ULXs in M 51 is well described by a single spectral component, *XMM-Newton* spectrum of most ULXs in NGC 5194 require at least two spectral components.

7.2.1. Cool accretion disks

X-ray spectra of two ULXs, sources 9 and 69, require soft components, modeled by either *mekal plus* MCD or two *mekal* components. The MCD components suggest inner disk temperatures of $kT_{in} \sim 130$ eV (source 9) and ~ 170 eV (source 69). These temperatures are lower than that found for ULXs studied with *ASCA* (Makishima et al. 2000) and Galactic X-ray binaries, but are similar to that found for ULXs studied with *XMM-Newton* (Miller et al. 2003; Miller, Fabian, & Miller 2004; Dewangan et al. 2004). The *XMM-Newton* observation of M 51 supports the increasing trend that ULXs have cooler accretion disks than GBH binaries. The temperature of the innermost regions of an accretion disk is given by

$$kT_{in} \approx 1.2 \text{ keV} \left(\frac{\xi}{0.41} \right)^{1/2} \left(\frac{\kappa}{1.7} \right) \alpha^{-1/2} \left(\frac{\dot{M}}{\dot{M}_E} \right)^{1/4} \left(\frac{M}{10 M_\odot} \right)^{-1/4} \quad (1)$$

(see e.g., Makishima et al. 2000). Here $\kappa \simeq 1.7$ is a spectral hardening factor. The factor $\xi \simeq 0.4$ takes into account the fact that the radius of maximum temperature is larger than the innermost stable orbit, and $\alpha = 1$ for a Schwarzschild geometry or $1/6$ for a Kerr geometry. Thus objects with lower MCD temperatures must have either higher black hole masses or lower accretion rates. Assuming a relative accretion rate of $\frac{\dot{M}}{\dot{M}_{Edd}} \sim 0.1$, equation 1 implies black hole masses of $\sim 7300 M_\odot$ (source 9) and $\sim 2500 M_\odot$ (source 69).

The results of the CMCD model fit to the spectrum of source 26 suggests that this ULX has cool accretion disk ($kT = 291_{-82}^{+13}$ eV). Using the normalization and the

inclination angle of CMCD model, it is possible to derive a BH mass as detailed in Wang et al. (2004). Using this procedure, we derive a black hole mass of $\sim 2800M_{\odot}$ for the ULX sources 26.

7.2.2. ULXs with a power-law spectrum

The X-ray spectrum of two ULXs, source 82 and source 12, can be described by a simple power-law models with a photon indices of ~ 2.4 and ~ 1.7 , respectively. Source 12 does not show any signature of emission from an accretion disk. The power-law spectral form of this ULX is similar to that of XRBs in their low state (Terashima & Wilson 2004) or type 1 AGNs (excluding the narrow-line Seyfert 1 galaxies). If the above analogy is correct, then the ULXs with simple power-law spectrum may imply very high mass ($>$ a few times $100M_{\odot}$) black hole. A power-law spectrum may also result from beamed X-ray emission. The X-ray spectrum of source 82 is very steep and may be similar to that of Galactic XRBs in their very high state (see Terashima & Wilson 2004 and Roberts et al. 2004 for a detailed discussion on the power-law spectral form of ULXs). It is also possible that ULXs with a simple power-law spectrum are background AGNs.

7.2.3. Spectral variability

It is not possible to compare directly the best-fit spectral form derived from the *Chandra* and *XMM-Newton* observations due to the different number of spectral components used to fit the spectra. Therefore, we compare the best-fit model derived from the *Chandra*, usually a single component model, and the corresponding single component model best-fit to the *XMM-Newton* data. The single component model is not necessarily the best-fit model to the *XMM-Newton* data. Figure 11 compares the spectral parameters illustrating the spectral variability of ULXs in M 51. The steeper spectrum of source 5 during the *XMM-Newton* observation may be due to the contribution of the soft source NGC 5194#6 detected with *Chandra* (see section 6.1). Source 9 shows a very soft X-ray spectrum and is consistent with no spectral shape variability. The detection of the power law component in addition to the soft component in the spectra of source 9 may be due to the larger collecting area of *XMM-Newton* particularly at higher energies. Sources 26, 37, 63 and 12 do not show significant variability in their spectral shape. Sources 41 and 82 show slightly steeper X-ray spectra compared with the earlier *Chandra* observation.

Source 69 continues to show drastic spectral and flux variability. The source was in a high/hard state (power law $\Gamma = 1.24^{+0.12}_{-0.17}$ or MCD $kT = 2.3^{+1.0}_{-0.5}$) in June 2000 and subsequently made a transition to an extremely soft/low state (power law $\Gamma > 5.1$ or MCD $kT = 0.17^{+0.13}_{-0.06}$) in June 2001 (Terashima & Wilson 2004). The ULX made another transition back to a state similar to its earlier high/hard state, in January 2003. The spectral transitions of source 69 are completely different from the high/soft to low/hard spectral transitions usually observed from Galactic XRBs but similar to those observed from some ULXs (The Antennae, Fabbiano et al. 2003; Holmberg II X-1, Dewangan et al. 2004; an ULX in NGC 7714, Soria & Motch 2004). The ULXs that show distinct spectral transitions may comprise a

distinct class of ULXs. The physics of these transitions is yet to be understood clearly.

7.2.4. Periodicity

Source 69 is the only ULX in M 51 that shows indications for a possible periodic variations in its X-ray flux. The periods detected from our *XMM-Newton* observation ($P = 5925 \pm 200$ s at a $\sim 2\sigma$ level) and the first *Chandra* observation ($P = 7620 \pm 500$ s) are significantly different. The two observations are separated by ~ 1.5 yrs. The variation in period, if real, clearly argues against orbital periodicity, and suggests the presence of quasi-periodic oscillations. Liu et al. (2002) discussed the possibility that the observed periodicity is due to orbital variations and as noted by Liu et al. (2002), only low mass X-ray binaries (LMXBs) can have orbital periods as small as 2 hr with high luminosities. In this case Liu et al. (2002) estimate the mass of the donor to be $\simeq 0.23M_{\odot}$. The spectrum of source 69 derived from the first *Chandra* observation was found to be consistent with an absorbed multicolor disk model with inner disk temperature of $kT = 2.10^{+0.63}_{-0.40}$ keV and showed marginal improvement in the fit after including a single temperature blackbody component. Based on these results, Liu et al. (2002) do not rule out the possibility that source 69 is a neutron star. Our *XMM-Newton* spectra require three components - a power-law ($\Gamma \sim 1.2$), a *mekal* ($kT \sim 680$ eV) and another *mekal* ($kT \sim 180$ eV) or a cool accretion disk ($kT_{in} \sim 170$ eV). The stellar mass black hole systems and high luminosity neutron star binary systems, both have high disk temperatures ($kT = 1 - 2$ keV). The possible variation in the period, due to a QPO and the X-ray spectrum both are inconsistent with the LMXB picture. Moreover, source 69 resides in a region that is likely to be undergoing active star formation, making it likely that the ULX is a high mass X-ray binary (HMXB). The spectral transition of source 69 from a high-hard to low-soft state also is in disagreement with the behavior of most Galactic LMXBs (Terashima & Wilson 2004).

If we interpret the variation of the apparent periodicity as resulting from QPOs, then QPO frequency of ~ 0.15 mHz is much lower than 67 mHz QPO observed with *RXTE* from the Galactic black hole candidate GRS 1915+105, which has a dynamically measured mass of $14 \pm 4M_{\odot}$ (Morgan, Remillard & Greiner 1997). The only ULX known to show QPO is M 82 X-1 (Strohmayer & Mushotzky 2003). Its QPO frequency of 54 mHz is also lower than that of GRS 1915+105 but much larger than the implied frequency for source 69. It is not necessary the case that QPO frequency scales with the mass of the black hole, only twin peak QPOs with a frequency ratio of 3:2 have been established to scale with black hole mass (McClintock & Remillard 2003). The micro-quasar GRS 1915+105 is known to show QPOs at kHz as well as mHz frequencies, the lowest frequency of QPO observed from GRS 1915+105 is 1.6 mHz (Morgan et al. 1997). Therefore it is not entirely unlikely the possibility of a ~ 0.15 mHz QPO from source 69. Long observations are required to clarify the presence of periodicity or QPO in this ULX.

8. CONCLUSIONS

We have analyzed *XMM-Newton* EPIC observation of M 51 performed in January 2003. Our main findings are

as follows:

- We detected 9 ULXs, an LLAGN and extended soft thermal emission from M 51. One of the sources (source 63) is a new ULX, not identified earlier due to its previously faint flux levels.
- All eight ULXs in NGC 5194 are located in or near spiral arms. Four ULXs are located in the regions of strong UV emission in the spiral arms, suggesting association of these ULXs with current star formation.
- Two ULXs (sources 26 and 69) show evidence for short-term variability. Source 69 is the most rapidly variable ULX in M 51 and shows a possible period of ~ 5925 s. All the ULXs except NGC 5194#12, show long-term variability by a factors of few to several.
- Most ULXs in M 51 show soft X-ray excess emission, above a hard power law, that is modeled by a *mekal* plasma and/or an MCD component. However the strength of the soft excess emission inferred from an ULX is comparable to the diffuse emission around individual ULXs excluding source 69. Thus the soft excess emission is unlikely to be physically associated with any of the ULXs except source 69. The soft excess emission from source 69

is about a factor four stronger than the surrounding diffuse emission and is likely intrinsic to the ULX.

- There is an indication of either a moderately broad ($\sigma = 100$ eV) iron $K\alpha$ line or an iron K absorption edge both due to neutral iron in the spectrum of source 26.
- The X-ray spectrum of LLAGN in NGC 5194 is extremely flat ($\Gamma \sim 0.7$) and shows a strong ($EW \sim 2.5$ keV), narrow, iron line from neutral material. The X-ray emission from the LLAGN in NGC 5194 is dominated by reflection from cold material.

We are grateful to an anonymous referee for the valuable comments and suggestions that improved the paper. This work is based on observations obtained with *XMM-Newton*, an ESA science mission with instruments and contributions directly funded by ESA member states and the USA (NASA). GCD acknowledges the support of NASA grant through the award NNG04GN69G. REG acknowledges NASA award NAG5-9902 in support of his Mission Scientist position on *XMM-Newton*. This research has made use of data obtained from the High Energy Astrophysics Science Archive Research Center (HEASARC), provided by NASA's Goddard Space Flight Center.

REFERENCES

- Arnaud, K. A. et al. 1985, MNRAS, 217, 105
 Begelman, M. C. 2002, ApJ, 568, L97
 Colbert, E. J. M. & Mushotzky, R. F. 1999, ApJ, 519, 89
 Colbert, E. J. M. & Ptak, A. F. 2002, ApJS, 143, 25
 Cropper, M., Soria, R., Mushotzky, R. F., Wu, K., Markwardt, C. B., & Pakull, M. 2004, MNRAS, 349, 39
 Deutsch, E. W., Margon, B. & Anderson, S. F. 2000, ApJ, 530, L31
 Dewangan, G. C., Miyaji, T., Griffiths, R. E., & Lehmann, I. 2004, ApJ, 608, L57
 Ehle, M., Pietsch, W., & Beck, R. 1995, A&A, 295, 289
 Fabbiano, G. & Trinchieri, G. 1987, ApJ, 315, 46
 Fabbiano, G. 1989, ARA&A, 27, 87
 Fabbiano, G., King, A. R., Zezas, A., Ponman, T. J., Rots, A., & Schweizer, F. 2003, ApJ, 591, 843
 Feldmeier, J. J., Ciardullo, R., & Jacoby, G. H. 1997, ApJ, 479, 231
 Filippenko, A. V. & Sargent, W. L. W. 1985, ApJS, 57, 503
 Fukazawa, Y., Iyamoto, N., Kubota, A., Matsumoto, Y., & Makishima, K. 2001, A&A, 374, 73
 Ho, L. C., Filippenko, A. V., Sargent, W. L. W., & Peng, C. Y. 1997, ApJS, 112, 391
 Horne, J. H. & Baliunas, S. L. 1986, ApJ, 302, 757
 Immler, S., Pietsch, W., & Aschenbach, B. 1998, A&A, 331, 601
 Jansen, F. et al. 2001, A&A, 365, L1
 Jenkins, L. P., Roberts, T. P., Warwick, R. S., Kilgard, R. E., & Ward, M. J. 2004, MNRAS, 349, 404
 King, A. R., Davies, M. B., Ward, M. J., Fabbiano, G., & Elvis, M. 2001, ApJ, 552, L109
 Kohno, K., Kawabe, R., Tosaki, T., & Okumura, S. K. 1996, ApJ, 461, L29
 Levenson, N. A., Krolik, J. H., Życki, P. T., Heckman, T. M., Weaver, K. A., Awaki, H., & Terashima, Y. 2002, ApJ, 573, L81
 Lira, P., Ward, M., Zezas, A., Alonso-Herrero, A., & Ueno, S. 2002, MNRAS, 330, 259
 Liu, J., Bregman, J. N., Irwin, J. & Seitzer, P. 2002, ApJ, 581, L93
 Magdziarz, P., & Zdziarski, A. A. 1995, MNRAS, 273, 837
 Morgan, E. H., Remillard, R. A., & Greiner, J. 1997, ApJ, 482, 993
 Makishima, K., Ohashi, T., Kondo, H., Palumbo, G. G. C., & Trinchieri, G. 1990, ApJ, 365, 159
 Makishima, K., et al. 2000, ApJ, 535, 632
 Marston, A. P., Elmegreen, D., Elmegreen, B., Forman, W., Jones, C., & Flanagan, K. 1995, ApJ, 438, 663
 Miller, J. M., Fabbiano, G., Miller, M. C., & Fabian, A. C. 2003, ApJ, 585, L37
 Miller, J. M., Fabian, A. C., & Miller, M. C. 2004, ApJ, 607, 931
 Mirabel, I. F. & Rodríguez, L. F. 1999, ARA&A, 37, 409
 Miyaji, T., Griffiths, R. E., Lumb, D., Sarajedini, V., & Siddiqui, H. 2003, Astronomische Nachrichten, 324, 24
 Palumbo, G. G. C., Fabbiano, G., Trinchieri, G., & Fransson, C. 1985, ApJ, 298, 259
 Protassov, R., van Dyk, D. A., Connors, A., Kashyap, V. L., & Siemiginowska, A. 2002, ApJ, 571, 545
 Roberts, T. P., Warwick, R. S., Ward, M. J., & Goad, M. R. 2004, MNRAS, 349, 1193
 Roberts, T. P., Goad, M. R., Ward, M. J., & Warwick, R. S. 2003, MNRAS, 342, 709
 Roberts, T. P., Warwick, R. S., Ward, M. J., & Murray, S. S. 2002, MNRAS, 337, 677
 Roberts, T. P. & Warwick, R. S. 2000, MNRAS, 315, 98
 Scargle, J. D. 1982, ApJ, 263, 835
 Stark, A. A., Gammie, C. F., Wilson, R. W., Bally, J., Linke, R. A., Heiles, C., & Hurwitz, M. 1992, ApJS, 79, 77
 Strohmayer, T. E. & Mushotzky, R. F. 2003, ApJ, 586, L61
 Strüder, L. et al. 2001, A&A, 365, L18
 Swartz, D. A., Ghosh, K. K., Tennant, A. F., & Wu, K. 2004, ArXiv Astrophysics e-prints, astro-ph/0405498
 Snowden, S. L., 2002, astro-ph/0203311.
 Soria, R., & Motch, C. 2004, A&A, 422, 915
 Stauffer, J. R. 1982, ApJ, 262, 66
 Terashima, Y., Ptak, A., Fujimoto, R., Itoh, M., Kunieda, H., Makishima, K., & Serlemitsos, P. J. 1998, ApJ, 496, 210
 Terashima, Y. & Wilson, A. S. 2001, ApJ, 560, 139
 Terashima, Y. & Wilson, A. S. 2004, ApJ, 601, 735
 Turner, M. J. L. et al. 2001, A&A, 365, L27
 Wang, Q. D., Yao, Y., Fukui, W., Zhang, S. N., & Williams, R. 2004, ApJ, 609, 113
 Yao, Y., Zhang, S. N., Zhang, X., Feng, Y., & Robinson, C. R. 2005, ApJ, 619, 446
 Zezas, A., Fabbiano, G., Rots, A. H., & Murray, S. S. 2002, ApJ, 577, 710
 Zezas, A., Ward, M. J., & Murray, S. S. 2003, ApJ, 594, L31

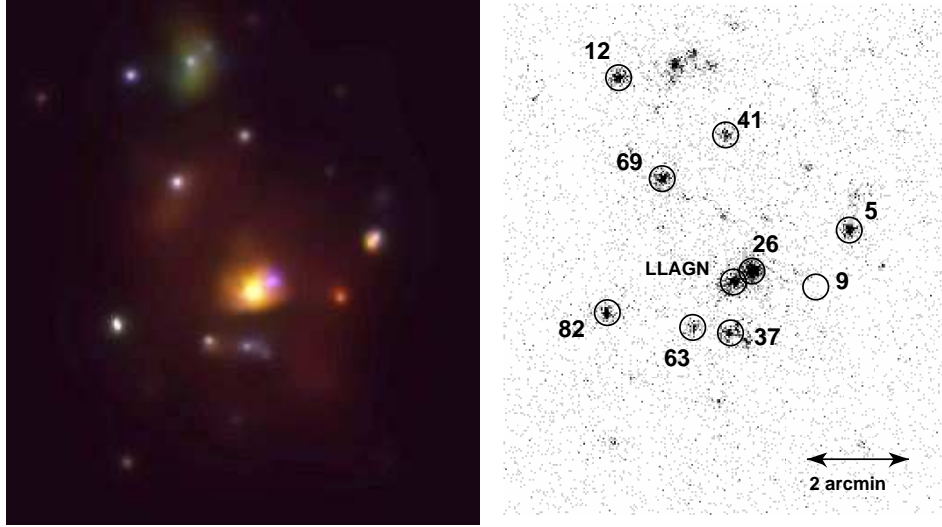


FIG. 1.— *Left*: Three color image of M 51 created from adoptively smooth *XMM-Newton* EPIC PN images. The three colors red, green, and blue correspond to the 0.2 – 0.7 keV, 0.7 – 2 keV, and 2 – 10 keV energy bands. North is towards the top and east is to the left of the image. The extended source at the top of the image is the companion galaxy NGC 5195. The bright extended source near the center of the image is the center of the galaxy NGC 5194 that consists of extended soft emission and two hard X-ray sources: the LLAGN and an ULX NGC 5194 source 26. *Right*: The EPIC PN image of M 51 in the 2 – 10 keV band showing the positions of 9 ULXs and the LLAGN.



FIG. 2.— *XMM-Newton* ultra-violet image overlaid with the 1.5 – 10 keV band X-ray contours, derived from the PN image, showing the discrete hard X-ray sources. The contours are drawn at levels of 0.4, 0.7, 1.3, 1.9, and 2.6 counts pixel⁻² (1 pixel = 0.953 arcsec). The image size 11.1' × 11.1'. North is up and east is left. Two central hard X-ray sources, about 20'' apart, are clearly resolved by the EPIC instruments. The center of UV image coincides with the fainter of the two hard X-ray sources in the central regions. This fainter source is the LLAGN in NGC 5194. The brighter source is the ULX NGC 5194 source 26.

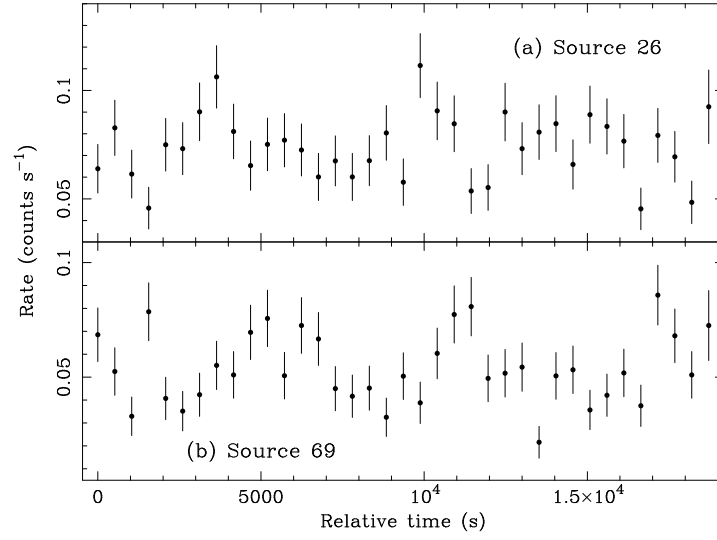


FIG. 3.— Short-term EPIC PN light curves of ULXs in M 51 (a) source 26, and (b) source 69. The bin sizes are 520 s. The light curves have been corrected for the background contribution.

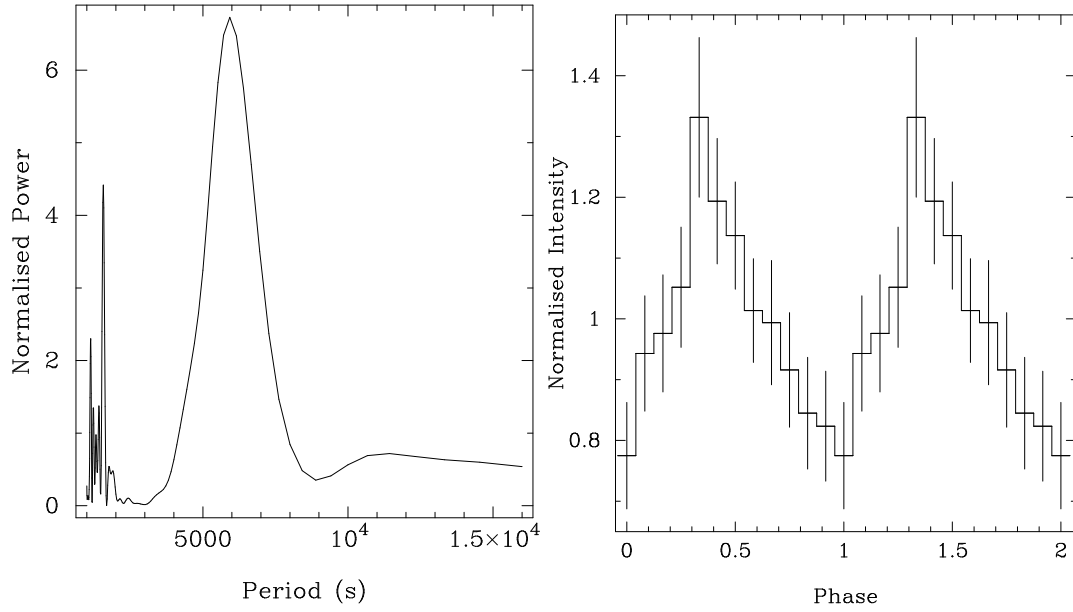


FIG. 4.— *Left*: Periodogram of NGC 5194 source 69. *Right*: Folded *XMM-Newton* light curve of NGC 5194 source 69.

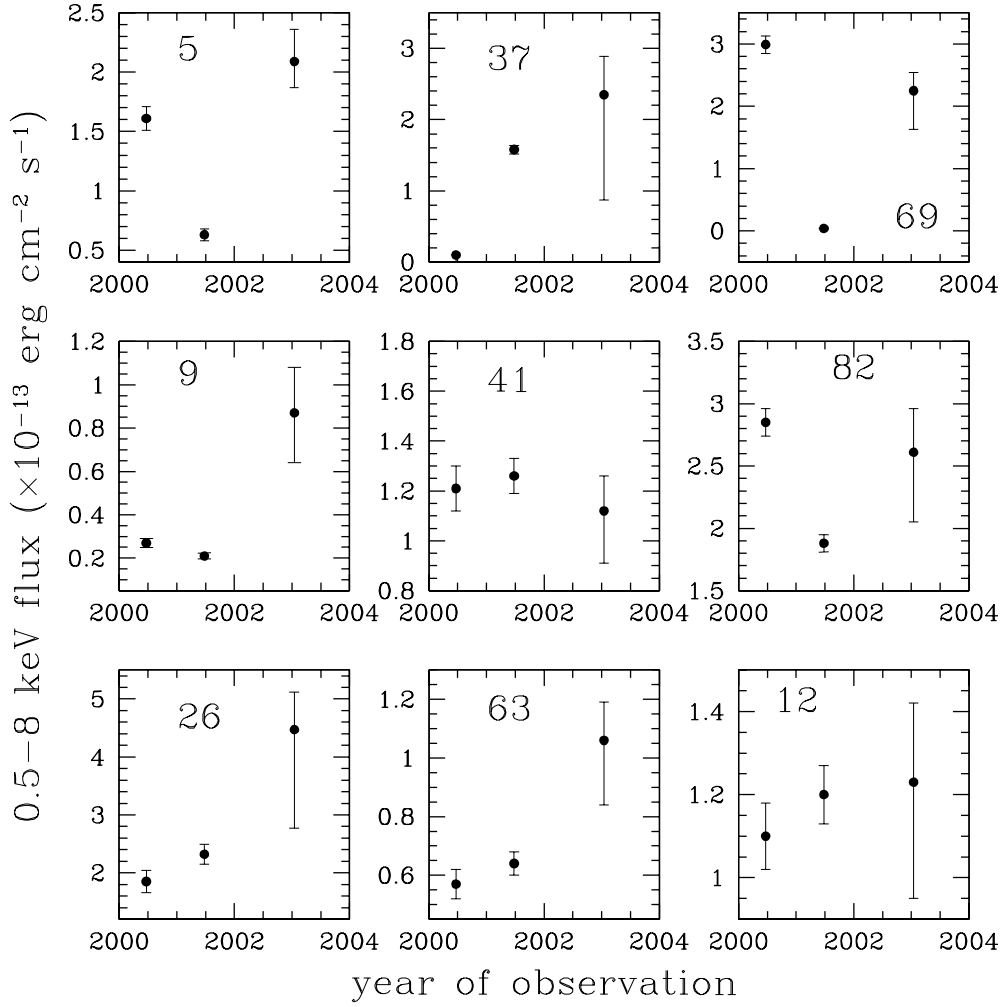


FIG. 5.— Long-term variability of ULXs in M 51 over a baseline of two and half years. The fluxes for the years 2000 and 2001 were derived from the two *Chandra* observations by Terashima & Wilson (2004). All but two ULXs 41 and 12 clearly varied.

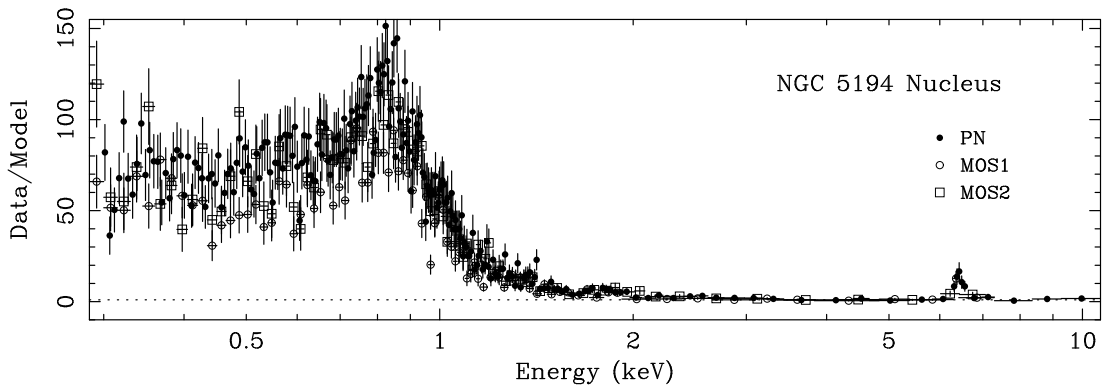


FIG. 6.— Ratio of the observed EPIC data and the best-fit power-law model obtained by fitting the data in the 3–6 keV and 7–10 keV bands.

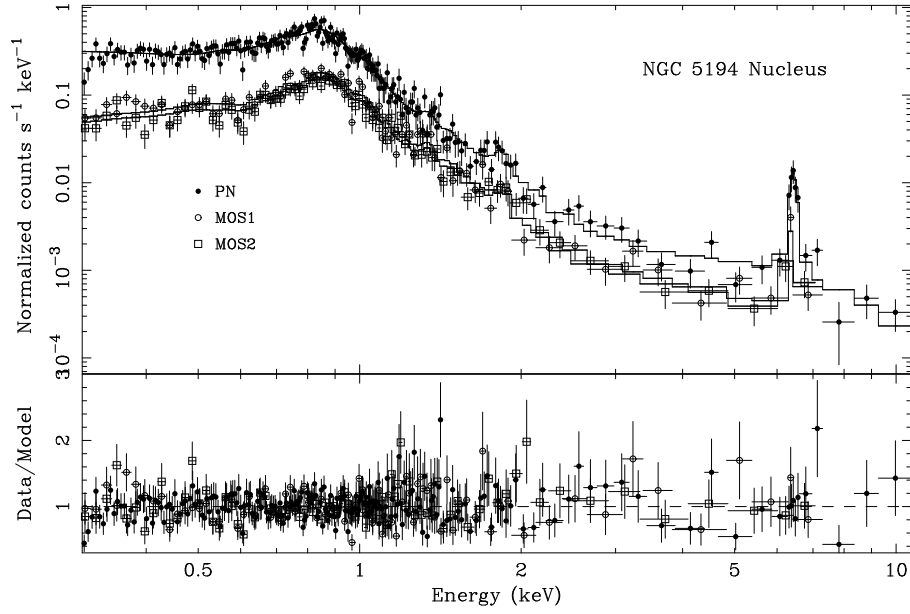


FIG. 7.— The observed EPIC PN and MOS spectra of the nucleus of NGC 5194 and the best-fitting spectral model which a combination of two *mekal* plasma components, power-law, and a narrow Gaussian line at 6.4 keV and multiplied by the Galactic absorption.

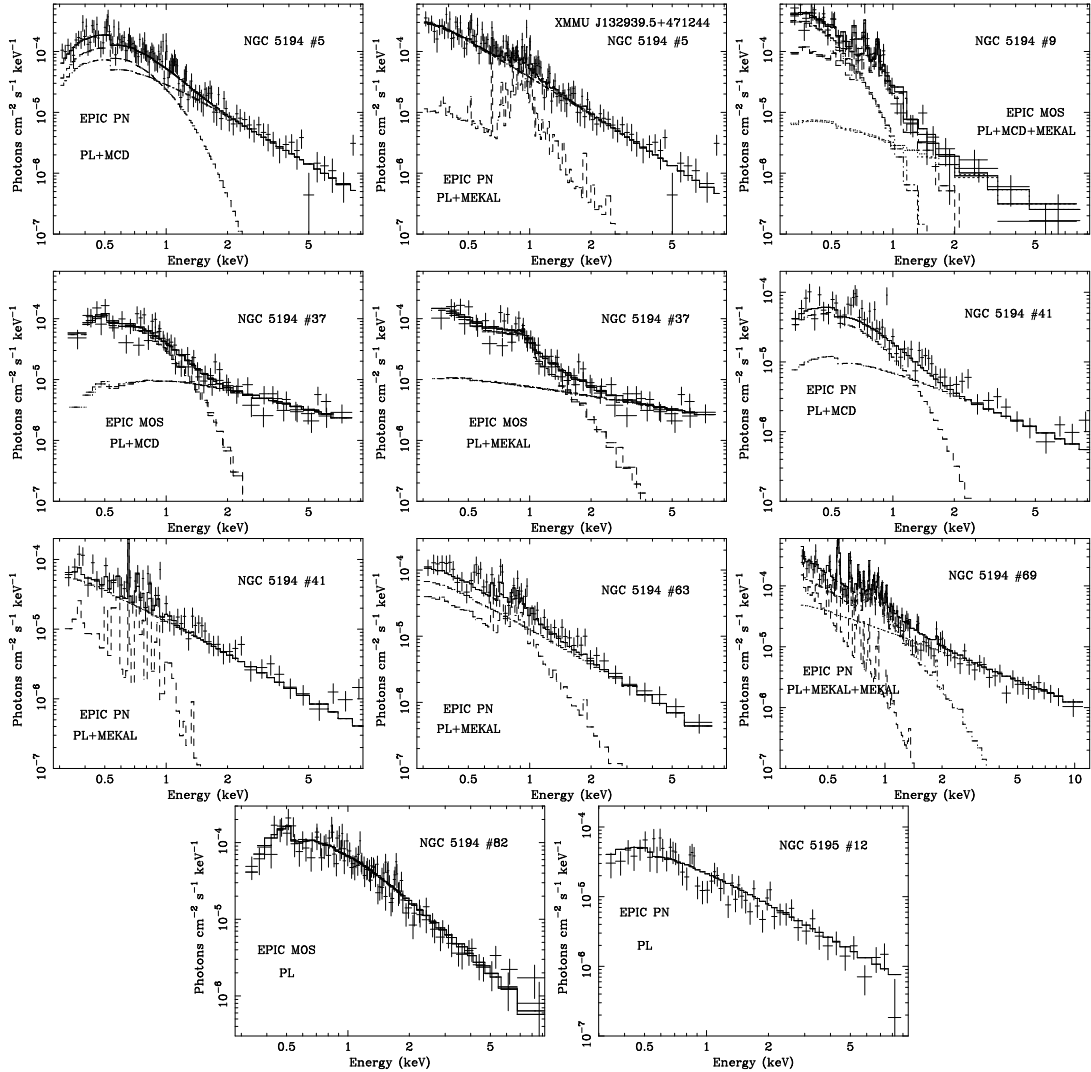


FIG. 8.— Unfolded EPIC PN or MOS spectra of ULXs in M51.

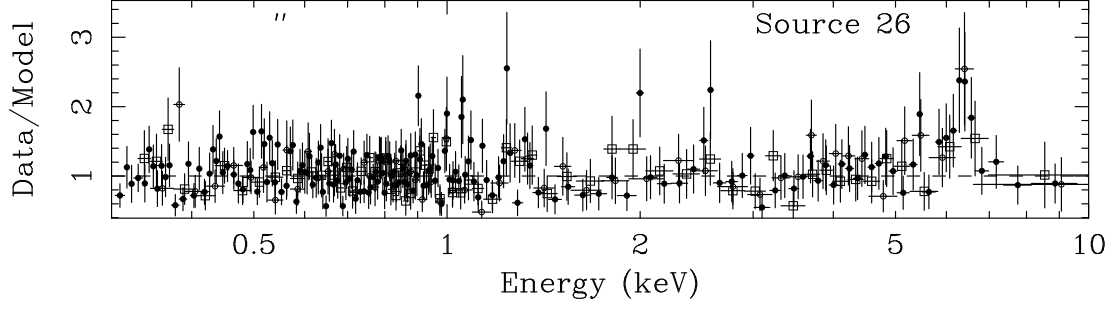


FIG. 9.— The ratio of the observed EPIC data and the best-fitting model consisting of three *mekal* components and a power law modified by the Galactic absorption. An iron $K\alpha$ line at 6.4 keV is evident. PN, MOS1, and MOS2 data are marked by filled circles, open circles, and open squares, respectively.

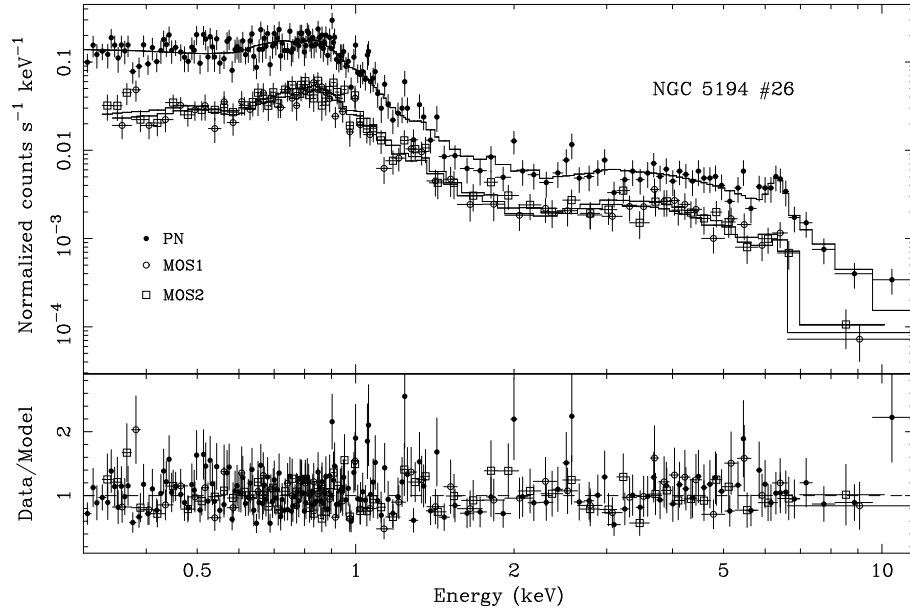


FIG. 10.— The observed EPIC PN and MOS spectra of the ULX NGC 5194#26 and the best-fitting spectral model – a combination of two *mekal* plasma components, a Gaussian line at ~ 6.4 keV, and an absorbed power-law.

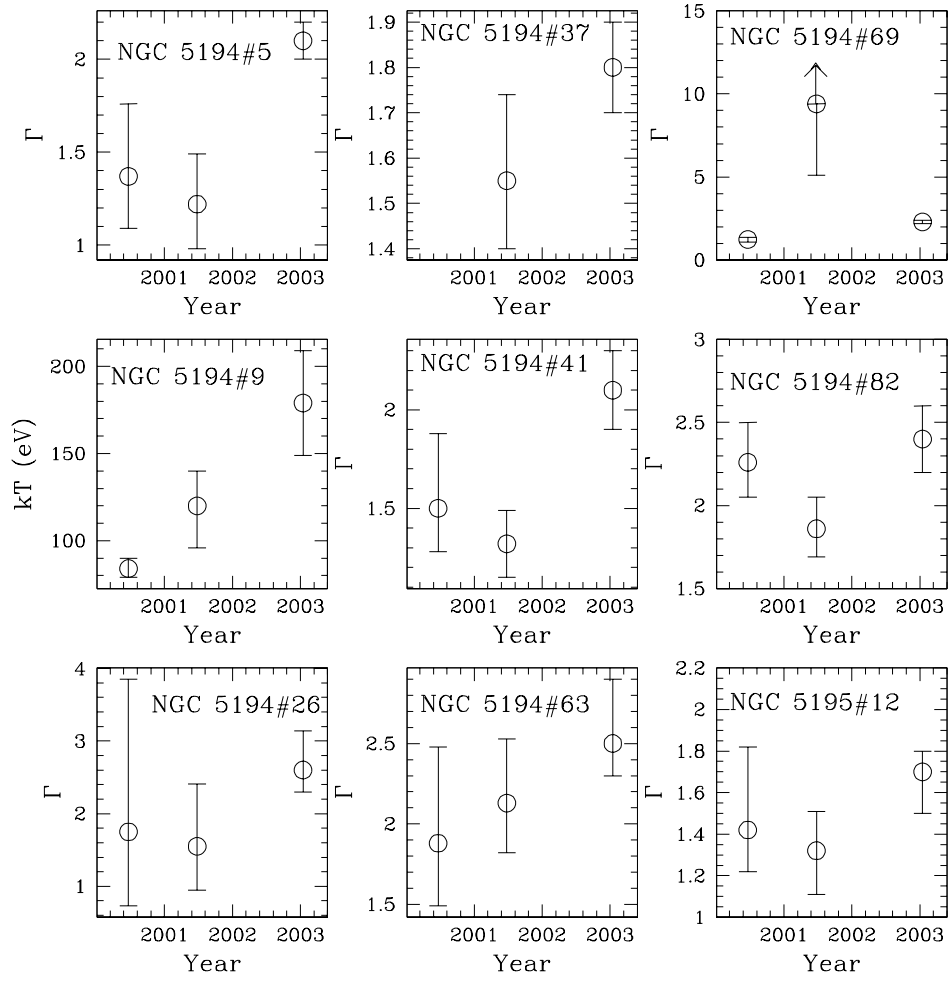


FIG. 11.— Long-term spectral shape variability of ULXs in M 51. The best-fit power-law models (for all ULXs but NGC 5194 source 9) and MCD model (for NGC 5194 source 9) to the *Chandra* data of June 2000 and June 2001, taken from Terashima & Wilson (2004), and to the *XMM-Newton* data of January 2003 have been used.

TABLE 1
THE LOW LUMINOSITY AGN AND LIST OF ULXs IN M 51

<i>Chandra</i> id	Host galaxy	<i>XMM-Newton</i> name XMMU	RA (2000)	Decl. (2000)	2 – 10 keV count rate (10^{-2} counts s $^{-1}$)		
					PN	MOS1	MOS2
LLAGN	NGC 5194	J132952.9+471140	13:29:52.87	+47:11:40.09	1.43 ± 0.09	0.46 ± 0.05	0.46 ± 0.05
5	NGC 5194	J132939.5+471241	13:29:39.55	+47:12:41.09	0.97 ± 0.09	0.38 ± 0.05	0.27 ± 0.04
9 ^a	NGC 5194	J132943.4+471134	13:29:43.37	+47:11:34.21	–	0.08 ± 0.03	0.05 ± 0.02
26	NGC 5194	J132950.7+471153	13:29:50.73	+47:11:52.86	2.40 ± 0.11	0.78 ± 0.06	0.82 ± 0.06
37 ^a	NGC 5194	J132953.3+471040	13:29:53.26	+47:10:40.23	–	1.64 ± 0.09	1.64 ± 0.09
41	NGC 5194	J132953.8+471433	13:29:53.77	+47:14:33.01	0.71 ± 0.06	0.17 ± 0.03	0.19 ± 0.03
63	NGC 5194	J132957.6+471047	13:29:57.56	+47:10:46.62	0.47 ± 0.05	0.18 ± 0.03	0.18 ± 0.03
69	NGC 5194	J133001.1+471342	13:30:01.090	+47:13:41.47	1.37 ± 0.09	0.40 ± 0.05	0.33 ± 0.04
82 ^a	NGC 5194	J133007.4+471104	13:30:07.407	+47:11:03.94	–	0.50 ± 0.05	0.49 ± 0.05
12	NGC 5195	J133006.1+471540	13:30:06.13	+47:15:40.20	0.83 ± 0.07	0.25 ± 0.04	0.27 ± 0.04

^aThese sources fall on the PN chip gaps. The coordinate was derived from the full band image.

TABLE 2
RESULTS OF SHORT-TERM VARIABILITY TESTS.

Source	χ^2 statistic		
	count rate (count s $^{-1}$)	χ^2/dof	P_{χ^2} (var)
5	$0.063^{+0.002}_{-0.002}$	29.29/36	–
9	$0.044^{+0.001}_{-0.001}$	42.88/36	–
26	$0.070^{+0.002}_{-0.002}$	57.28/36	98.64%
37	$0.053^{+0.002}_{-0.002}$	41.66/36	–
41	$0.023^{+0.001}_{-0.001}$	46.29/36	–
63	$0.034^{+0.001}_{-0.001}$	30.77/36	–
69	$0.049^{+0.002}_{-0.002}$	70.91/36	99.95%
82	$0.074^{+0.002}_{-0.002}$	42.23/36	–
12	$0.025^{+0.001}_{-0.001}$	38.19/36	–

TABLE 3
RESULTS OF THE JOINT SPECTRAL FITTINGS TO THE EPIC PN AND MOS SPECTRA OF M 51 NUCLEUS

Component	Parameter	model 1 ^a	model 2 ^a	model 3 ^a
absorption	N_H cm ⁻²	1.57×10^{20} (f)	1.57×10^{20} (f)	1.57×10^{20} (f)
<i>mekal</i>	kT (eV)	171^{+23}_{-29}	603^{+16}_{-17}	177^{+36}_{-32}
	Abundance (solar)	$0.20^{+2.49}_{-0.14}$	—	$0.20(f)$
	O	—	$0.08^{+0.07}_{-0.06}$	—
	Ne	—	$0.18^{+0.07}_{-0.07}$	—
	Mg	—	$0.10^{+0.05}_{-0.05}$	—
	Si	—	$0.12^{+0.06}_{-0.05}$	—
	S	—	$0.32^{+0.29}_{-0.22}$	—
	Ar	—	$1.47^{+1.28}_{-1.08}$	—
	Ca	—	$2.38^{+3.14}_{-1.07}$	—
	Fe	—	$0.11^{+0.02}_{-0.01}$	—
	Ni	—	< 0.17	—
	$norm^c$	$2.0^{+4.2}_{-1.4} \times 10^{-4}$	$1.2^{+0.1}_{-0.1} \times 10^{-3}$	$1.9^{+0.6}_{-0.3} \times 10^{-4}$
<i>mekal</i>	kT (eV)	610^{+16}_{-14}	—	614^{+13}_{-11}
	Abundance	$0.18^{+0.05}_{-0.02}$	—	$0.18(f)$
	$norm^c$	$7.6^{+1.7}_{-1.3} \times 10^{-4}$	—	$7.8^{+0.3}_{-0.3} \times 10^{-4}$
Power law	Γ	$0.43^{+0.34}_{-0.33}$	$0.2^{+0.3}_{-0.4}$	—
	norm	$4.1^{+1.5}_{-1.7} \times 10^{-6}$	$2.7^{+1.9}_{-1.3} \times 10^{-6}$	—
pexrav	Γ	—	—	$1.9(f)$
	R	—	—	$1.0(f)$
	i (degree)	—	—	$70(f)$
	norm	—	—	$2.1^{+0.3}_{-0.2} \times 10^{-4}$
Gaussian	E (keV)	$6.43^{+0.03}_{-0.03}$	$6.43^{+0.02}_{-0.03}$	$6.43^{+0.02}_{-0.03}$
	σ (eV)	61^{+42}_{-51}	62^{+42}_{-50}	$10(f)$
	f_{line}^d	$4.7^{+1.1}_{-1.0}$	$4.74^{+1.14}_{-1.00}$	$4.6^{+0.9}_{-1.1}$
	EW (keV)	2.6	2.6	2.5
Total	$f(0.3 - 10 \text{ keV})^e$	8.2	8.2	8.2
	$L(0.3 - 10 \text{ keV})^f$	6.9	6.9	6.9
	$f(2 - 10 \text{ keV})^e$	2.1	1.9	2.0
	$L(2 - 10 \text{ keV})^f$	1.8	1.6	1.7
	C/dof	414.7/401	414.7/396	420.9/400
	Goodness of fit	47.8%	46.9%	61.8%

^a(f) indicates a fixed parameter.

^bModel 1 is a combination of two *mekal*, a power-law, a narrow Gaussian multiplied the Galactic absorption model. Model 2 is the same as model 1 except that the two *mekal* components have been replaced by a *vmekal* component. Model 3 is the same as model 1 with the power-law replaced by a neutral reflection model *pexrav*.

^cIn units of $10^{-14} \frac{1}{4\pi d^2} \int n_e n_H dV$, where d is the angular size distance to the source (cm), n_e is the electron density (cm⁻³), and n_H is the hydrogen density (cm⁻³).

^dLine flux in units of 10^{-6} photons cm⁻² s⁻¹.

^eObserved flux in units of 10^{-13} erg cm⁻² s⁻¹.

^fObserved luminosity in units of 10^{39} erg s⁻¹.

TABLE 4

BEST-FIT SPECTRAL MODEL PARAMETERS DERIVED FROM THE JOINT PN/MOS DATA FOR THE ULXs IN M 51. THE FLUXES MEASURED WITH THE PN AND MOS DATA ARE SIMILAR WITHIN ERRORS, AND THE QUOTED FLUXES ARE FROM THE PN DATA ONLY.

ULX	Model ^a	N_H^b 10^{20} cm^{-2}	F (eV)	kT_{MCD} (eV)	kT_{mekal} (eV)	f_X^d	L_X^e	C/dof	GOF	$\Delta C/\Delta p^f$	MLR significance
5	A	$8.6^{+2.6}_{-2.3}$	$2.5^{+0.2}_{-0.1}$	—	—	—	—	234.6/206	76.4%	—	—
	B	1.57(f)	—	485^{+28}_{-26}	—	—	—	400.5/207	100.0%	—	—
	C	$9.1^{+4.4}_{-4.5}$	$2.0^{+0.2}_{-0.1}$	210^{+45}_{-7}	—	$2.1^{+0.3}_{-0.2}$	$1.8^{+0.2}_{-0.2}$	213.3/204	34.2%	-21.3/2	2.4×10^{-5}
	D	1.57(f)	$2.0^{+0.1}_{-0.1}$	—	802^{+106}_{-111}	$2.0^{+0.2}_{-0.2}$	$1.7^{+0.2}_{-0.2}$	210.5/205	42.1%	-24.1/1	9.1×10^{-7}
9 ^c	A	$28.6^{+15.4}_{-10.0}$	$5.7^{+1.3}_{-0.8}$	—	—	—	—	113.7/54	99.8%	—	—
	B	$8.3^{+8.4}_{-6.2}$	—	163^{+29}_{-26}	—	—	—	110.7/54	92.3%	—	—
	C	$28.4^{+19.8}_{-13.8}$	$2.0^{+0.8}_{-0.7}$	107^{+28}_{-25}	—	$1.0^{+0.4}_{-0.5}$	$0.8^{+0.3}_{-0.5}$	69.5/52	72.9%	-44.2/2	2.5×10^{-10}
	D	1.57(f)	$3.3^{+0.5}_{-0.5}$	—	290^{+62}_{-30}	$0.9^{+0.2}_{-0.2}$	$0.7^{+0.2}_{-0.2}$	72.9/53	89.3%	-40.8/1	1.7×10^{-10}
37 ^c	E	$1.6^{+1.8}_{-1.6}$	$1.4^{+0.7}_{-0.8}$	130^{+36}_{-50}	349^{+61}_{-42}	$0.9^{+0.2}_{-0.2}$	$0.8^{+0.2}_{-0.2}$	59.8/50	46.9%	-53.9/4	5.5×10^{-11}
	F	1.57(f)	$1.6^{+1.0}_{-0.8}$	—	$80^{+35}_{-44}, 306^{+62}_{-39}$	$1.0^{+0.3}_{-0.2}$	$0.8^{+0.2}_{-0.2}$	67.9/51	78.2%	-45.8/3	6.2×10^{-10}
	A	1.57(f)	$1.7^{+0.1}_{-0.1}$	—	—	—	—	104.9/61	99.9%	—	—
	B	1.57(f)	—	1253^{+156}_{-131}	—	—	—	232.8/61	100.0%	—	—
41	C	$12.4^{+15.9}_{-11.0}$	$0.8^{+0.4}_{-0.5}$	220^{+125}_{-67}	—	$2.3^{+0.4}_{-1.1}$	$1.9^{+0.3}_{-0.9}$	68.6/58	57.9%	-36.3/3	6.5×10^{-8}
	D	1.57(f)	$0.8^{+0.3}_{-0.5}$	—	691^{+170}_{-94}	$2.3^{+0.5}_{-1.5}$	$1.9^{+0.5}_{-1.2}$	65.2/59	65.2	-39.7/2	2.4×10^{-9}
	A	1.57(f)	$1.8^{+0.1}_{-0.1}$	—	—	—	—	169.1/129	96.3%	—	—
	B	1.57(f)	—	1134^{+94}_{-82}	—	—	—	392.7/129	100.0%	—	—
63	C	$4.2^{+11.2}_{-4.2}$	$1.2^{+0.3}_{-0.3}$	272^{+88}_{-100}	—	$1.1^{+0.2}_{-0.5}$	$1.0^{+0.2}_{-0.4}$	143.8/126	59.8%	-25.3/3	1.3×10^{-5}
	D	1.57(f)	$1.5^{+0.1}_{-0.2}$	—	341^{+86}_{-73}	$1.1^{+0.1}_{-0.2}$	$0.9^{+0.1}_{-0.2}$	146.6/127	69.6%	-22.5/2	1.3×10^{-5}
	A	$5.4^{+2.8}_{-2.7}$	$2.3^{+0.1}_{-0.2}$	—	—	—	—	137.0/101	97.0%	—	—
	B	1.57(f)	—	788^{+55}_{-47}	—	—	—	376.8/102	100.0%	—	—
69	C	$3.9^{+10.0}_{-3.9}$	$1.5^{+0.5}_{-0.4}$	283^{+100}_{-105}	—	$1.1^{+0.2}_{-0.5}$	$0.9^{+0.2}_{-0.4}$	116.3/99	65.7%	-20.3/2	3.9×10^{-5}
	D	1.57(f)	$1.8^{+0.2}_{-0.2}$	—	608^{+28}_{-149}	$1.1^{+0.2}_{-0.2}$	$0.9^{+0.1}_{-0.2}$	105.1/100	42.60%	-31.9/1	1.6×10^{-8}
	A	1.57(f)	$2.1^{+0.1}_{-0.1}$	—	—	—	—	342.0/204	100.0%	—	—
	B	1.57(f)	—	891^{+42}_{-39}	—	—	—	1091.3/204	100.0%	—	—
82 ^c	C	$12.6^{+7.0}_{-4.5}$	$1.3^{+0.2}_{-0.2}$	190^{+28}_{-31}	—	$2.3^{+0.3}_{-0.8}$	$1.9^{+0.2}_{-0.7}$	220.0/201	67.3%	-122.0/3	2.8×10^{-26}
	D	1.57(f)	$1.6^{+0.1}_{-0.1}$	—	368^{+44}_{-52}	$2.2^{+0.2}_{-0.3}$	$1.8^{+0.2}_{-0.2}$	244.6/202	87.6%	-106.4/2	7.8×10^{-24}
	E	$5.2^{+8.8}_{-5.2}$	$1.2^{+0.2}_{-0.2}$	169^{+73}_{-44}	689^{+105}_{-73}	$2.2^{+0.3}_{-0.6}$	$1.9^{+0.2}_{-0.5}$	200.9/199	29.2%	-141.1/5	1.0×10^{-28}
	F	1.57(f)	$1.2^{+0.2}_{-0.2}$	—	$181^{+57}_{-47}, 676^{+112}_{-60}$	$2.3^{+0.3}_{-0.4}$	$1.9^{+0.2}_{-0.4}$	191.9/200	17.1%	-150.1/4	1.9×10^{-31}
12	A	$15.8^{+3.7}_{-3.7}$	$2.4^{+0.2}_{-0.2}$	—	—	$2.6^{+0.4}_{-0.4}$	$2.2^{+0.4}_{-0.4}$	98.3/100	32.4%	—	—
	B	1.57(f)	—	809^{+62}_{-56}	—	—	—	164.2.3/101	100.0%	—	—
	C	$7.4^{+8.2}_{-5.2}$	$1.4^{+0.6}_{-0.6}$	406^{+43}_{-20}	—	$2.7^{+0.1}_{-2.0}$	$2.3^{+0.1}_{-1.7}$	91.5/98	12.8%	-6.8/2	0.033
	D	$13.0^{+4.4}_{-4.3}$	$2.2^{+0.1}_{-0.2}$	—	727^{+360}_{-258}	$2.6^{+0.4}_{-0.6}$	$2.2^{+0.3}_{-0.5}$	93.7/98	21.3%	-4.6/2	0.100
12	A	$5.6^{+3.7}_{-3.5}$	$1.6^{+0.1}_{-0.1}$	—	—	$1.2^{+0.2}_{-0.3}$	$1.0^{+0.2}_{-0.3}$	88.4/93	21.3%	—	—
	B	1.57(f)	—	1290^{+140}_{-120}	—	—	—	121.5/98	92.2%	—	—
	G	1.57(f)	—	—	7930^{+2923}_{-1637}	$1.3^{+0.2}_{-0.3}$	$1.1^{+0.2}_{-0.2}$	87.7/94	18.7%	—	—

^aA= PL, B = MCD, C = PL+MCD, D = PL+mekal, E = PL+MCD+mekal, F=PL+mekal + mekal, G=mekal.

^bTotal absorption column density. The Galactic column is $1.5 \times 10^{20} \text{ cm}^{-2}$.

^cOnly MOS data were used for the spectral fitting. The source photons fall at the chip gap in the PN camera.

^dObserved flux in units of $10^{-13} \text{ erg cm}^{-2} \text{ s}^{-1}$ and in the energy band of 0.5 – 8 keV band.

^eObserved luminosity in units of $10^{39} \text{ erg s}^{-1}$ and in the energy band of 0.5 – 8 keV band.

TABLE 5
RESULTS OF THE JOINT SPECTRAL FITTINGS TO THE EPIC PN AND MOS SPECTRA OF THE ULX NGC 5194 SOURCE 26

Component	Parameter ^a	model 1 ^b	model 2 ^b
<i>mekal</i>	kT (eV)	253^{+84}_{-69}	251^{+86}_{-69}
	abundance (solar)	0.1(<i>f</i>)	0.1(<i>f</i>)
	$norm^c$	$1.8^{+1.2}_{-0.6} \times 10^{-4}$	$1.8^{+1.3}_{-0.6} \times 10^{-4}$
<i>mekal</i>	kT (eV)	589^{+74}_{-40}	589^{+75}_{-39}
	abundance (solar)	0.1(<i>f</i>)	0.1
	$norm^c$	$3.4^{+0.5}_{-1.2} \times 10^{-4}$	$3.4^{+0.5}_{-1.2} \times 10^{-4}$
absorption	N_H ($\times 10^{22}$ cm $^{-2}$)	$7.1^{+1.5}_{-1.4}$	$10.5^{+1.4}_{-4.2}$
power law	Γ	$2.45^{+0.39}_{-0.20}$	—
	$norm$	$3.9^{+3.7}_{-1.8} \times 10^{-4}$	—
Gaussian	E keV	$6.33^{+0.11}_{-0.13}$	$6.33^{+0.11}_{-0.12}$
	σ (eV)	158^{+180}_{-155}	170^{+167}_{-136}
	f	$2.3^{+1.5}_{-1.2} \times 10^{-6}$	$2.7^{+1.5}_{-1.3} \times 10^{-6}$
CMCD	EW (eV)	550	615
	kT_{in} (eV)	—	291^{+13}_{-82}
	kT_c (keV)	—	$50.0^{+35.7}_{-18.1}$
	R_c (R_g)	—	$6.65^{+3.2}_{-3.2}$
	τ	—	$2.0^{+3.0}_{-1.2}$
	i^d	—	$53.6^{+31.4p}_{-18.6p}$
	K^e	—	$143.9^{+383.9}_{-90.3}$
Total	$f_X (\times 10^{-13}$ erg cm $^{-2}$ s $^{-1}$) ^g	$4.47^{+0.65}_{-1.70}$	$4.47^{+3.20}_{-2.34}$
	$L_X (\times 10^{39}$ erg s $^{-1}$) ^g	$3.76^{+0.54}_{-1.42}$	$3.76^{+2.69}_{-1.96}$
	C/dof	278.5/295	275.0/291
	Goodness of fit	9.3%	10.6%

^a(*f*) indicates a fixed parameter.

^bModel 1 is a combination of two *mekal*, a power-law, a narrow Gaussian multiplied by an absorption model. Model 2 is same as model 1 except that the power-law has been replaced with the comptonized MCD model.

^cIn units of $10^{-4} \times 10^{-14} \frac{1}{4\pi d^2} \int n_e n_H dV$, where d is the angular size distance to the source (cm), n_e is the electron density (cm $^{-3}$), and n_H is the hydrogen density (cm $^{-3}$).

^dParameter pegged at both limits

^eCMCD normalization, $K = (\frac{R_{in}/km}{D/10 \text{ kpc}})$.

^gObserved flux and luminosity in the 0.5 – 8 keV band.

